

# A QCD SPACE-TIME ANALYSIS OF QUARKONIUM FORMATION AND EVOLUTION IN HADRONIC COLLISIONS

Klaus Geiger

*Physics Department, Brookhaven National Laboratory, Upton, NY 11973, USA*

e-mail: klaus@bnl.gov

The production of heavy quarkonium as  $Q\bar{Q}$  bound-states in hadron-hadron collisions is considered within the framework of a space-time description, combining parton-cascade evolution with a coalescence model for bound-state formation. The ‘hard’ production of the initial  $Q\bar{Q}$ , directly or via gluon fragmentation and including both color-singlet and color-octet contributions, is calculated from the PQCD cross-sections. The subsequent development of the  $Q\bar{Q}$  system is described within a space-time generalization of the DGLAP parton-evolution formalism in position- and momentum-space. The actual formation of the bound-states is accomplished through overlap of the  $Q\bar{Q}$  pair and a spectrum of quarkonium wave-functions. This coalescence can only occur after sufficient gluon radiation reduces the  $Q\bar{Q}$  relative velocity to a value commensurate with the non-relativistic kinematics of these bound systems. The presence of gluon participants in the cascade then is both necessary and leads to the natural inclusion of both color-singlet and color-octet mechanisms. The application of this approach to  $pp$  ( $p\bar{p}$ ) collisions from  $\sqrt{s} = 30$  GeV - 14 TeV reveals very decent agreement with available data from ISR and Tevatron - without the necessity of introducing fit parameters. Moreover, production probabilities are calculated for a complete spectrum of charmonium and bottonium states, with the relative significance compared to open charm (bottom) production. An analysis of the space-time development is carried through which sheds light on the relevance of gluon radiation and color-structure, suggesting a corresponding experimental investigation.

## I. INTRODUCTION

The experimental analysis of quarkonia production in high-energy particle collisions has brought in the last couple of years exciting discoveries, both in  $p + \bar{p}$  collisions at the Fermilab Tevatron [1], and in  $Pb + Pb$  collisions at the CERN SPS [2]. In the first case, the interpretation of the Tevatron data [3] of quarkonium production in  $p + \bar{p}$  at  $\sqrt{s} = 1800$  GeV, revealed a drastic disagreement with expectations from theoretical calculations that described lower-energy data very well. Not only was the quarkonium yield underestimated by a far more than an order of magnitude (in particular for  $J/\psi$  and  $\psi'$ ), but also the observed  $p_\perp$ -dependence of the cross-sections was very different from what was predicted earlier. This has become known as the ‘CDF anomaly’. In the second case, a significant suppression of  $J/\psi$  production observed in the CERN heavy-ion data [2] of  $Pb + Pb$  at  $E_{beam} = 158$  A GeV ( $\sqrt{s} = 17$  A GeV), implied that a naive extrapolation from experiments with lighter nuclei substantially overestimated the  $J/\psi$  production. Clearly, these two discoveries concerning quarkonium production, namely, ‘enhancement’ in  $p + \bar{p}$ , and ‘suppression’ in  $Pb + Pb$  have rather different origin. However, if one is to comprehend the underlying mechanisms in ion-ion applications from anything close to fundamental QCD, then both aspects have to be considered. In the case of  $p + \bar{p}$  (and also  $e^+e^-$ ) vital theoretical progress based on QCD’s first principles has been made [4,5] in the last few years. In the case of heavy-ion collisions the degree of theoretical insight is still perhaps more suspect, at present mainly covering ad-hoc prescriptions or somewhat oversimplified models, however with promising exceptions [6].

To set the stage, I recall that the recent achievements in understanding quarkonium production in hadronic collisions at high energy and momentum transfer were essentially stimulated by two ‘observations’ inferred from Tevatron data: First, gluon fragmentation (and not direct  $Q\bar{Q}$  production) appears to be the dominant source of prompt quarkonia at high energies, i.e., a process that involves the high- $p_\perp$  production of a virtual gluon, followed by its subsequent evolution and decay into  $Q\bar{Q}$ . Second, a substantial fraction of quarkonium production at very high energy arises from intermediate color-octet fluctuations during the evolution into a final-state color-singlet  $Q\bar{Q}$  pair, a contribution which is small at ISR energies but becomes very prominent at Tevatron energy and beyond.

Previous to these observations, calculations of charmonium production were limited to the use of the so-called color singlet model [7–9] (for a recent review of heavy quarkonium production, see [10]). A theoretical breakthrough was achieved by Bodwin, Braaten, and Lepage [11], who developed a rigorous QCD formalism by marrying Perturbative QCD (PQCD) and an effective field theory within Non-relativistic QCD (NRQCD). These authors combined in systematic manner the short-distance, relativistic physics of  $Q\bar{Q}$  production and evolution, with the non-perturbative, supposedly non-relativistic dynamics of the formation of hadronic  $Q\bar{Q}$  bound-states. This novel theory [12] exploited some unique features of the quarkonium bound-states. Firstly, the high- $p_\perp$  production of a  $Q\bar{Q}$  pair, directly by a hard parton collision or indirectly via gluon fragmentation, is a truly perturbative process with the heavy quark mass  $M_Q$  naturally bounding the typical momentum scale from below. Secondly, the internal  $Q\bar{Q}$  dynamics is inherently non-relativistic, since in order to have a finite probability for producing a  $Q\bar{Q}$  bound-state, the pair necessarily must have very small relative momentum, despite potentially large total momentum.

Quantitatively, an important ingredient is the presence in quarkonium physics of several energy (or momentum) scales, well separated if the relative velocity  $\mathbf{v}$  of the  $Q\bar{Q}$  satisfies  $|\mathbf{v}| \equiv v \ll 1$ . The three important scales [11,15] are (i) the heavy mass  $M_Q$ , setting the lower scale for the relativistic  $Q\bar{Q}$  production with typical momenta  $\gtrsim M_Q$  and small-size configurations  $\sim 1/M_Q$ , (ii) the momentum  $M_Q v$ , specifying the scale for bound-state formation with typical momenta  $\sim M_Q v$  and mean bound-state size  $\sim 1/M_Q v$ , and (iii) the kinetic energy  $M_Q v^2$ , which if small ensures that a nonrelativistic treatment of the bound-state may be reasonable [13,14]. If  $v \ll 1$  then  $M_Q \gg M_Q v \gg M_Q v^2$  and a double series expansion in the strong coupling  $\alpha_s$  and the velocity parameter  $v$  is meaningful. Since  $v \propto 1/\ln M_Q$ , typical values for the heavy quark velocities are  $v_{c\bar{c}} = 0.23$  and  $v_{b\bar{b}} = 0.08$ . Bodwin, Braaten, and Lepage [11] demonstrated that one may then really use PQCD to compute the various color-singlet and color-octet contributions of different  $Q\bar{Q}$  Fock state components to quarkonium production. The latter, however, are converted into formation probabilities for quarkonium only after multiplication by unknown non-perturbative matrix-elements for the  $Q\bar{Q}$  conversion into physical states. Nonetheless, it triggered several works addressing the application to  $e^+e^-$  physics [16] and  $p\bar{p}$  collisions [15,17]. In the context of aforementioned ‘CDF anomaly’, it was shown [15] that by estimating the color-singlet contributions from quarkonium potential models, and by fitting the color-octet contributions to experimental data, the addition of the *color-octet mechanism* can impressively resolve the disagreement of the  $p + \bar{p}$  Tevatron data with previous predictions within the *color-singlet model* only. \*

---

\* It should be noted that the so-called *color evaporation model* with an early history [18], was also capable of including octets but is too severely constrained by its assumptions [4] to have a useful applicability.

• color-singlet production

• color-octet mechanism

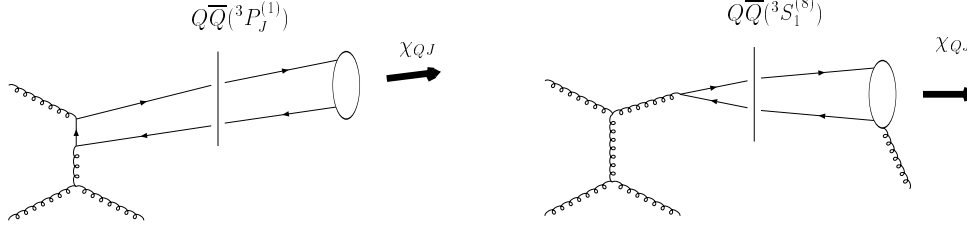


FIG. 1. Feynman graphs that contribute to  $\chi_{QJ}$  production at  $O(\alpha_s^3)$  through color-singlet and color-octet mechanisms. The initial  $Q\bar{Q}$  is produced in a  $^3P_J^{(1)}$  state, respectively a  $^3S_1^{(8)}$  state, at short distances and hadronizes into a final-state  $\chi_{QJ}$  bound-state at large distances.

Nonetheless, some critical remarks are at hand here. The dictates of experimental data aside, the physical justification of the color-octet mechanism remains unsatisfactory. To clarify this statement and to motivate the aims of this paper, it is useful to draw a somewhat idealistic picture, to be improved on later in this work, of color-singlet and color-octet  $Q\bar{Q}$  production in hadron-hadron collisions. In Fig. 1a a typical *color-singlet* Feynman graph that yields a  $\chi_{QJ}$  is depicted. The  $O(\alpha_s^3)$  hard scattering of the incoming partons produces at a short-distance scale an outgoing color-less  $Q\bar{Q}$  pair in a  $^3P_J^{(1)}$  state plus a gluon. The heavy  $Q$  and  $\bar{Q}$  fly out from the initial collision point, almost on mass-shell, eventually forming, at large distances, a hadronic  $\chi_{QJ}$  bound-state. In Fig. 1b, a *color-octet*  $Q\bar{Q}$  pair in a  $^3S_1^{(8)}$  state is created by the hard parton scattering, and the pair is assumed to color-neutralize far away from the collision point by emitting an extremely long-wavelength gluon which takes away the color, but virtually no energy or momentum. The heavy quark pair then may transform again into a  $\chi_{QJ}$  state.

Whereas the color-singlet production is clearly plausible, the color-octet mechanism seems to contradict basic quantum mechanics. The assumption that an ultra-soft gluon takes away the color, but virtually no energy or momentum is just wrong! Such a gluon cannot carry away any quantum numbers within a finite time. The emitted gluon must be sufficiently hard if it is to both neutralize the color-octet  $Q\bar{Q}$  and separate from the  $Q\bar{Q}$  as an individual and incoherent quantum before the  $Q\bar{Q}$  pair hadronizes. Since the typical formation time of a  $Q\bar{Q}$  bound-state is  $t_{form} \sim 1/M_{Q\bar{Q}} \gtrsim 1 \text{ fm}$ , the gluon must have at least an energy  $\omega_g = O(1 \text{ GeV})$  if it is emitted at early time, and even more if it is radiated later. Such a gluon is certainly not a long-distance fluctuation with negligible energy. Hence, although the intervention of the color-octet mechanism resolves the Tevatron data paradox, I am inclined to pose, provocatively, the question: Can the ad-hoc motivation of the color-octet mechanism not be extended towards a more physically intuitive scheme, still consistent with the principles of PQCD and NRQCD? In fact, the probability of directly producing sufficiently low relative velocity  $Q\bar{Q}$  octet or singlet pairs for appreciable coalescence to occur is very small. Thus, in a model which attempts to combine both PQCD and NRQCD to generate quarkonium, moderately hard gluon radiation plays an integral part and both singlet and octet pairs enter straightforwardly. The gluon radiation serves to reduce the difference momentum to a point where coalescence is more probable, and of course automatically enables both singlet and octet mechanisms.

This is the very point where the work of this paper begins. Inspired by the above discussion, I take steps towards a ‘microscopic’ space-time QCD description of heavy quarkonium production. The ‘hard’ production of the initial  $Q\bar{Q}$ , directly or via gluon fragmentation and including both color-singlet and -octet contributions, is calculated from the PQCD cross-sections. The subsequent development of the  $Q\bar{Q}$  system is described within a space-time generalization of the DGLAP parton-evolution formalism [19,20] in position- and momentum-space. The actual formation of the bound-states is accomplished through overlap of the  $Q\bar{Q}$  pair and a spectrum of quarkonium wave-functions.

The analysis in this paper is confined to  $pp$  ( $p\bar{p}$ ) collisions in the energy range  $\sqrt{s} = 30 \text{ GeV} - 14 \text{ TeV}$ , spanned by ISR, Tevatron and LHC beam energies. Once the space-time structure of quarkonium production in ‘clean’  $pp$  ( $p\bar{p}$ ) collisions has been better understood, one may step further to address the observed quarkonium suppression in ‘dirty’ heavy-ion collisions, where the space-time information of  $Q\bar{Q}$  evolution in and interaction with the nuclear medium is most essential.

In the approach that I advocate here and hope to present in a convincing way in the remainder, it is very natural to incorporate both color-octet and color-singlet mechanisms. A produced  $c\bar{c}$  pair can start in either color state, although of course they form charmonium only in the singlet. As I shall show, gluon radiation plays so dominant a role in the final coalescence into a bound-state that both singlet and octet states must be involved during the  $p\bar{p}$  or  $pp$  evolution. At the same time it is of great importance to estimate the unknown non-perturbative effects, embodied in the conversion probabilities, from a dynamic coalescence picture [21] originally constructed for the production of deuterons from neutron and proton constituents of nuclear collisions.

The very explicit cascade space-time structure, for say a  $p\bar{p}$  collision, permits testing for coalescence after repeated gluon emission from a heavy quark pair. The qualitative picture that underlies the present phenomenological approach is inspired by the above-mentioned combination of PQCD and NRQCD. Accordingly, I also assume that the genealogy of a heavy  $Q\bar{Q}$  bound-state hadron involves three, in space-time well-separated components: first, the production of an initial  $Q\bar{Q}$  pair (directly or via gluon fragmentation), second, its subsequent evolution into a final-state  $Q\bar{Q}$  pair, and third, the conversion of the  $Q\bar{Q}$  pair into a bound-state hadron  $H_{Q\bar{Q}}$ . Imagine a heavy  $Q\bar{Q}$  pair emerging from a hard process of large momentum transfer scale, with relative probability given by the appropriate hard QCD cross-sections. This initial off-shell  $Q\bar{Q}$  pair, color-singlet or color-octet, then propagates in space-time according to relativistic cascading, and simultaneously, but subject to the uncertainty principle, evolves in momentum space according to the DGLAP evolution equations that describe the transmutation to the final-state color-singlet  $Q\bar{Q}$  in terms of real and virtual gluon emission. Finally, the probability for the  $Q\bar{Q}$  pair to form a hadronic bound-state  $H_{Q\bar{Q}}$  is assumed to be given by the overlap of the  $Q$  and  $\bar{Q}$  wave-functions with the bound-state wave-function. I will discuss and examine each of these three, essentially factorizable, building blocks of the model in detail.

This novel approach to quarkonium production and bound-state formation brings improvements on three distinct levels when compared to previous work based on combining (lowest order) PQCD matrix-elements with heavy quark effective theory in NRQCD:

1. A *dynamical cascade description* is employed that allows to trace the detailed history of the evolution in both space-time and momentum space, from the instant of initial  $Q\bar{Q}$  production, through the propagation and cascading of the pair and its gluonic offspring, and up to the formation of the final bound-state hadron.

This is to be seen in strong contrast to the previous calculations, which commonly were of a *static* nature, in the sense that no reference was made to the microscopic time-development of the quarkonium system. Nor were attempts made to account for ‘real’ gluon emission or possible rescattering of the quark-antiquark composite during its evolution. In the present approach on the other hand, the evolution is governed by the dynamics itself, including both ‘deterministic’ gluon emission processes and ‘statistical’ scattering or absorption processes. The space-time history is followed causally and provides at any given time the trajectories, coordinates and interaction vertices of the particles.

2. The *PQCD aspects* of the quarkonia were in earlier work described in terms of lowest order perturbative matrix-elements for the production of a quark-antiquark pair in a given state of angular momentum, spin and color-singlet or color-octet [3,4]). It was assumed that the initially produced  $Q\bar{Q}$  and the final bound-state forming  $Q\bar{Q}$  were identical states during the perturbative evolution, except for the (in some works) included momentum scale dependence. Thus, there was no chance for the initial pair to change its spin or color state after being produced by the emission of one or more perturbative gluons.

In contrast, the present approach allows the initial  $Q\bar{Q}$  to be produced statistically in any spin and color combination and then to change its state by gluon emission, absorption or scattering. Thus, the final  $Q\bar{Q}$  quantum state can be altered and the eventual yield of bound-state hadrons is a statistical outcome of the cascade development. Further, matrix-element calculations, though in principle exact, are in practice limited to first and second order in PQCD, suffering from the technical complications that enter with increasing order in perturbation theory. The cascade description, on the other hand, is based on the DGLAP equations. In principle the entire series expansion in  $\alpha_s$  is included by resummation, although admittedly in an approximate fashion and limited to the leading log approximation. Many observables in high-energy  $e^+e^-$  or  $p\bar{p}$  collisions, for which even second order matrix-elements calculations are insufficient, are reproduced with high accuracy in the parton cascade description [22].

3. The probability for the *non-perturbative conversion* of the final state  $Q\bar{Q}$  state into a bound-state hadron  $H_{Q\bar{Q}}$  with specific total angular momentum  $J$ , orbital angular momentum  $L$  and total spin  $S$  has been modeled throughout the literature by simply lumping all non-perturbative dynamics into the value of the bound-state (radial) wave-function  $\mathcal{R}_0(r)$  for  $L = 0$  (or its derivative  $\mathcal{R}'_1(r)$  for  $L = 1$ ) at zero  $Q\bar{Q}$  separation  $r \equiv |\mathbf{r}_Q - \mathbf{r}_{\bar{Q}}| = 0$ . The underlying motivation for this approximation is borrowed from positronium annihilation, assuming that the bound-state hadron emerges from the annihilation of  $Q$  and  $\bar{Q}$ , and that the probability for  $Q\bar{Q} \rightarrow H_{Q\bar{Q}}$  may be approximated by the wave-function behavior uniquely at (or near) the origin. Not only does this approach neglect the finite width of the bound-state wave-function, but also implies that the probability given by  $\mathcal{R}_0$  or  $\mathcal{R}'_1$  is independent of time, hence independent of the actual spatial  $Q\bar{Q}$  configuration along time-dependent trajectories for the  $Q$  and  $\bar{Q}$ .

In the present approach these shortcomings are absent, since it enables to evaluate at any given time the probability for  $Q\bar{Q} \rightarrow H_{Q\bar{Q}}$  as a function of both relative separations  $r$  and relative momentum  $k$  of the  $Q$  and  $\bar{Q}$ ,

using the full expression for the wave-function overlap integral (admittedly, model wave-function), rather than simply rely on the value of the wave-function at zero  $r$ . This might be termed a dynamic coalescence picture. Moreover, I do not interpret the conversion process as  $Q\bar{Q}$  annihilation, but as a coalescence process, analogously to, e.g., deuteron production in nuclear physics. Simple but effective techniques have been developed and tested in the literature [21], which I adopt and apply to the present problem.

The remainder of the paper is organized as follows. Sec. II is devoted to introducing the theoretical framework corresponding to the qualitative picture drawn above. Based on the factorization assumption of short-distance PQCD production and evolution of heavy  $Q\bar{Q}$  pairs, and the long-distance coalescence process with bound-state formation, the total squared amplitude for quarkonium production in hadronic collisions is obtained as the product of three functions corresponding to  $Q\bar{Q}$  production, parton cascade evolution, and coalescence, respectively. It is outlined how the resulting quarkonium cross-section can be calculated by simulating the space-time development of the complete particle system of a collision event with Monte Carlo methods as implemented in the computer program VNI [23]. In Sec. 3 the formalism is then specifically applied to  $pp$  ( $p\bar{p}$ ) collisions in the energy range  $\sqrt{s} = 30$  GeV - 14 TeV, corresponding to center-of-mass energies between ISR, Tevatron, and LHC experiments. Comparison with experimental data from ISR and Tevatron for both charmonium and bottomonium production is made, and the underlying dynamics specific to the model calculations, is examined in detail, in particular with respect to the relevance of gluon radiation, the contributions of color-singlet and color-octet  $Q\bar{Q}$  systems, and the characteristics of the space-time structure. Sec. 4 is reserved for concluding remarks and a brief discussion of future perspectives of the model, especially with respect to application to heavy-ion collisions and the issue of quarkonium suppression in dense nuclear matter.

## II. HEAVY QUARK PRODUCTION, EVOLUTION & COALESCENCE TO BOUND-STATES

Focus of interest is the production of quarkonium states  $H_{Q\bar{Q}}$  with definite quantum numbers  $J, L, S$  on both the charm and bottom sector, for which the following nomenclature is employed:

$$H_{c\bar{c}}(^{2S+1}L_J) = \begin{cases} \eta_c (^1S_0) \\ J/\psi (^3S_1) \\ h_c (^1P_1) \\ \chi_{c0} (^3P_0) \\ \chi_{c1} (^3P_1) \\ \chi_{c2} (^3P_2) \end{cases} \quad H_{b\bar{b}}(^{2S+1}L_J) = \begin{cases} \eta_b (^1S_0) \\ \Upsilon (^3S_1) \\ h_b (^1P_1) \\ \chi_{b0} (^3P_0) \\ \chi_{b1} (^3P_1) \\ \chi_{b2} (^3P_2) \end{cases} . \quad (1)$$

Following the outline of Sec. 1, the total amplitude for the production of a quarkonium hadron  $H_{Q\bar{Q}}$  in a collision of beam particles  $A, B$  may be written as a factorized ansatz. As schematically illustrated in Fig. 2, the relevant amplitude can then be represented as a product of three components:

- (i) the short-distance perturbative amplitude for production of a time-like fluctuation, being either an off-shell heavy pair  $c^* = Q\bar{Q}$  or a virtual gluon  $c^* = g$ , plus associated initial-state gluon- and  $q\bar{q}$ -production in a hard collision of partons in the incoming beam particles  $A, B$  (e.g.  $p, \bar{p}$ ) with large momentum transfer  $Q^2 \gg \Lambda^2$ ;
- (ii) the perturbative evolution of the produced fluctuation  $c^*$  into a final-state color-singlet  $[Q\bar{Q}]^{JLS(1)}$  pair with definite total spin  $S$ , relative and total angular momentum  $L$  and  $J$ , either by  $Q\bar{Q} \rightarrow [Q\bar{Q}]^{JLS(1)}$  (*direct production*), or by  $g \rightarrow [Q\bar{Q}]^{JLS(1)}$  (*gluon fragmentation*), in both cases accompanied by emission of other gluons and  $q\bar{q}$  pairs;
- (iii) the long-distance non-perturbative amplitude for the conversion of the final-state color-singlet  $[Q\bar{Q}]^{JLS(1)}$  assumed to occur by coalescence, into a bound-state hadron  $H_{Q\bar{Q}}(^{2S+1}L_J)$ , as categorized by (1).

Hence, the formula for this factorized ansatz can be expressed as

$$\begin{aligned} \mathcal{A}(AB \rightarrow H_{Q\bar{Q}} + X) = & \mathcal{A}(AB \rightarrow c^* + n g + n' q + \bar{n}' \bar{q})_{production} \\ & \times \mathcal{A}(c^* \rightarrow [Q\bar{Q}]^{JLS(1)} + m g + m' q + \bar{m}' \bar{q})_{evolution} \\ & \times \mathcal{A}([Q\bar{Q}]^{JLS(1)} \rightarrow H_{Q\bar{Q}}(^{2S+1}L_J))_{coalescence} , \end{aligned} \quad (2)$$

where  $ng, n'q, \bar{n}'\bar{q}$  etc., are the additional gluons and anti-quarks, respectively, being emitted from the incoming and outgoing partons of the hard vertex, and during the cascade evolution (c.f. Fig.2).

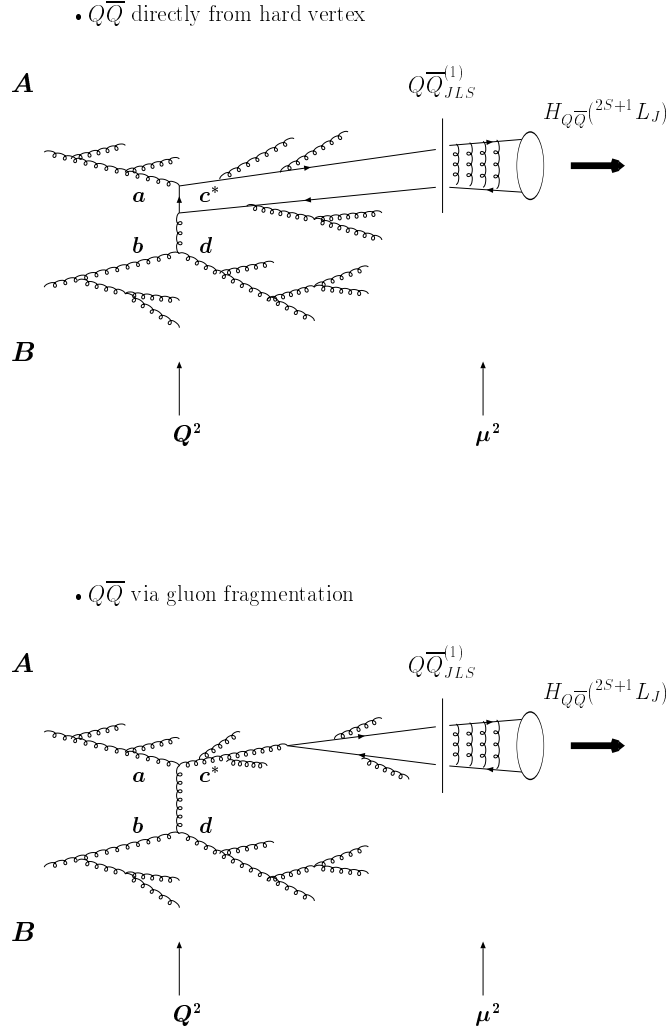


FIG. 2. Schematics of quarkonium production in the present approach: An initial  $Q\bar{Q}$  pair is produced by a hard collision  $ab \rightarrow c^*d$  where  $c^* = Q\bar{Q}$  (direct production) or  $c^* = g$  with subsequent  $g \rightarrow Q\bar{Q}$  (gluon fragmentation). The PQCD evolution includes real and virtual radiative processes off the incoming and outgoing partons. The coalescence of the resulting final  $Q\bar{Q}$  pair yields a bound-state hadron  $H_{Q\bar{Q}}$  with specific quantum numbers  $J, L, S$ .

In order to compute physical observables such as the total production cross-section, one needs to calculate the square of the amplitude (2). On account of the above factorization assumption, interference between the three subamplitudes is ignored, and therefore the total squared amplitude becomes a product of three squared subamplitudes, each of which may be interpreted probabilistically. Henceforth, I denote these squared subamplitudes by

- (i)  $\mathcal{P}_{c^*}^2$  for the production process resulting in  $c^* = Q\bar{Q}$ , or  $c^* = g$  with  $g \rightarrow Q\bar{Q}$ ,

(ii)  $\mathcal{E}_{c^*}^2$  for the perturbative evolution in space-time and momentum space,

(iii)  $\mathcal{C}_{JLS}^2$  for the coalescence mechanism and formation of a bound-state  $H_{Q\bar{Q}}^{(2S+1)L_J}$ .

Indicating in their arguments the relevant momentum and space-time variables, one can therefore express the square of (2) as follows:

$$\begin{aligned} |\mathcal{A}(AB \rightarrow H_{Q\bar{Q}} + X)|^2 &\equiv |\mathcal{A}(s, Q^2 | k_1, k_2, \bar{\mathbf{r}}_1, \bar{\mathbf{r}}_2, t)|^2 \\ &= \sum_{c^*=g, Q\bar{Q}} \mathcal{P}_{c^*}^2(\mu^2, Q^2, s | \bar{\mathbf{R}}_0, t_0) \times \mathcal{E}_{c^*}^2(Q^2, \mu^2 | k_1, k_2, \bar{\mathbf{r}}_1, \bar{\mathbf{r}}_2, t) \times \mathcal{C}_{JLS}^2(\mu^2 | k_1, k_2, \bar{\mathbf{r}}_1, \bar{\mathbf{r}}_2, t) . \end{aligned} \quad (3)$$

The quantity  $Q^2$  characterizes the hard scale at the production vertex,  $\mu^2 = O(1\text{-}2 \text{ GeV})$  is the mass scale that marks the boundary between perturbative and non-perturbative regimes, and  $\sqrt{s}$  is the center-of-mass energy of the colliding beam particles  $A, B$ . The four-momenta and mean trajectories of the  $Q$  and  $\bar{Q}$ , respectively, are defined by

$$k_i^\mu = (k_i^0, \mathbf{k}_i) \quad r_i^\mu = (r_i^0, \mathbf{r}_i) \quad \bar{\mathbf{r}}_i = \langle \mathbf{r}_i(t) \rangle , \quad (4)$$

where  $i = 1, 2$  for  $Q$  and  $\bar{Q}$ , respectively, and,

$$t = \frac{1}{2} (r_1^0 + r_2^0) \quad \bar{\mathbf{R}}_0 = \frac{1}{2} (\bar{\mathbf{r}}_1 + \bar{\mathbf{r}}_2)_{t=t_0} \quad (5)$$

is the time  $t$ , referring to the specific Lorentz frame in which one wishes to describe the dynamical evolution, while  $t_0$  and  $\bar{\mathbf{R}}_0$  labels the point of time and mean position at which the hard collision occurs.

Separate discussions of the three functions  $\mathcal{P}^2$ ,  $\mathcal{E}^2$  and  $\mathcal{C}^2$  are assigned to the next three subsections. The total production cross-section for quarkonium mesons of type  $H_{Q\bar{Q}}$  is then obtained, in Section IID, by summing over all contributing channels and multiplying (3) with the proper flux- and phase-space factors.

### A. Production

The square of the production amplitudes  $\mathcal{A}(AB \rightarrow g^* + n g + n' q + \bar{n}' \bar{q})_{production}$  in (3) gives the probability for materializing a time-like fluctuation  $c^* = Q\bar{Q}$  or  $c^* = g$  with  $k^2 \approx Q^2$  in a hard collision of partons  $a, b = g, q, \bar{q}$  at the hard scale  $Q^2$  set by the momentum transfer at the hard vertex. As illustrated in Fig. 3, the squared amplitude can be calculated from the usual  $2 \rightarrow 2$  hard-scattering amplitudes for  $ab \rightarrow c^* d$ , multiplied by the space-like Sudakov formfactors  $S_{a,b}$  for the incoming partons  $a$  and  $b$  and the time-like formfactor  $T_d$  for the outgoing parton  $d$ , resumming the contributions of real and virtual gluon radiation. The initial-state partons are weighted with the parton structure functions  $f_{a/A}$  and  $f_{b/B}$  of the beam particles  $A, B$ . Hence, the production probability is

$$\begin{aligned} \mathcal{P}_{c^*}^2(\mu^2, Q^2, s | \bar{\mathbf{R}}_0, t_0) &\equiv \left| \mathcal{A}(AB \rightarrow c^* + n g + n' q + \bar{n}' \bar{q})_{production} \right|^2 \\ &= \sum_{ab} \int dx_a \int dx_b f_{a/A}(x_a, \mu^2) S_a(x_a, \mu^2, Q^2 | t_0) f_{b/B}(x_b, \mu^2) S_b(x_b, \mu^2, Q^2 | t_0) \\ &\quad \times |A(ab \rightarrow c^* d)|^2(\hat{s}, Q^2 | \bar{\mathbf{R}}_0, t_0) \times T_d(Q^2, \mu^2 | t_0) . \end{aligned} \quad (6)$$

where the sum is over all contributing parton channels, and the hard collision  $ab \rightarrow c^* d$  is assumed to occur at time  $t_0$  and mean position  $\bar{\mathbf{R}}_0 = \langle \bar{\mathbf{R}}_0 \rangle$ . Furthermore,

$$s = (P_A + P_B)^2 \quad \mu^2 \gtrsim 1 \text{ GeV}^2 \quad Q^2 \equiv p_\perp^2 . \quad (7)$$

are, in that order, the total center-of-mass energy squared, the factorization scale that marks the perturbative boundary below which the non-perturbative dynamics is absorbed in the structure-functions, and the momentum transfer scale at the hard vertex of the colliding partons  $a, b$ , set by the relative transverse momentum of the outgoing parton jets. The Mandelstam variables at the parton level,  $\hat{s}, \hat{t}, \hat{u}$ , and the lightcone fractions  $x_{a,b}$  of the colliding partons  $a, b$  are defined as usual

$$\hat{s} = x_a x_b s \quad \hat{t} = -x_b p_\perp \sqrt{s} e^{y_2} \quad \hat{u} = -x_a p_\perp \sqrt{s} e^{y_2} \quad x_{a,b} = \frac{(k_0 + k_z)_{a,b}}{\sqrt{s}} , \quad (8)$$

where the incoming parton momenta are parametrized as

$$k_a^\mu = x_a \frac{\sqrt{s}}{2} (1, 0, 0, 1) \quad k_b^\mu = x_b \frac{\sqrt{s}}{2} (1, 0, 0, -1) , \quad (9)$$

while the momenta of the scattered parton  $c^*$  and of the recoiling parton  $d$ , with corresponding jet rapidities  $y_1$  and  $y_2$  are, respectively,

$$k_{c^*}^\mu = p_\perp (\cosh y_1, 1, 0, \sinh y_1) \quad k_d^\mu = p_\perp (\cosh y_2, -1, 0, \sinh y_2) . \quad (10)$$

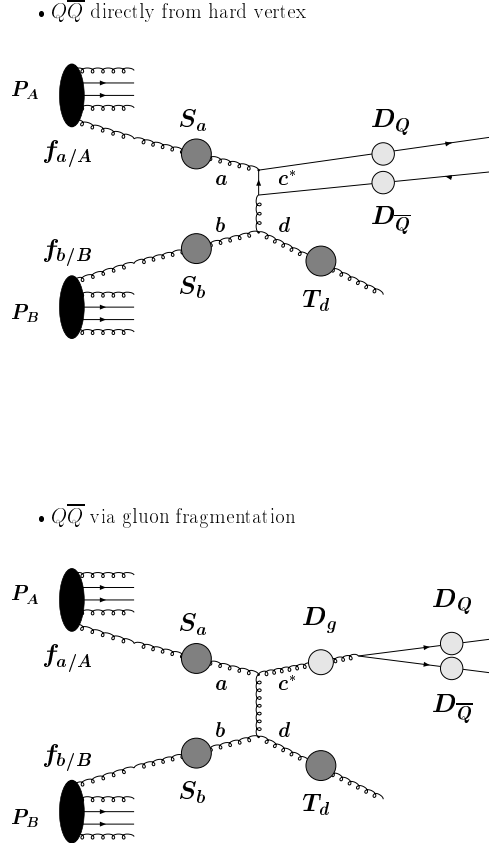


FIG. 3. Graphical representation of the amplitude for the production and evolution of a  $Q\bar{Q}$  pair, analogous to Fig. 2: the usual  $2 \rightarrow 2$  hard-scattering amplitudes for  $ab \rightarrow c^*d$  are multiplied by the space-like Sudakov formfactors  $S_{a,b}$  for the incoming partons  $a$  and  $b$  and the outgoing parton  $d$  is dressed by a time-like formfactor  $T_d$ , which contain the resummation of real and virtual gluon emission. Similarly, the functions  $D_g, D_Q, D_{\bar{Q}}$  embody the PQCD evolution of outgoing gluon- $Q\bar{Q}$  system. The initial state is weighted with the parton structure-functions  $f_{a/A}$  and  $f_{b/B}$  of the beam particles  $A, B$ .

The elementary hard process in (6)  $ab \rightarrow c^*d$ , where  $a, b = g, q, \bar{q}$ , involves the PQCD matrix-elements for producing a  $Q\bar{Q}$  with definite color and angular momentum quantum numbers to  $O(\alpha_s^3)$ . These matrix-elements have been calculated for both color-singlet [8,9] and color-octet [15] contributions for a spectrum of  $Q\bar{Q}$  states. The explicit, rather complicated expressions are well documented in the quoted references. It is however useful to plot in Fig. 4 the magnitudes and dependence with momentum transfer of the partonic cross-sections, which are related to the squared matrix-elements as usual by  $d\hat{\sigma}/d\hat{t} = 1/(16\pi\hat{s}^2) |A(ab \rightarrow c^*d)|^2(\hat{s}, \hat{t})$ . The Feynman diagrams that contribute to order  $O(\alpha_s^3)$  to these partonic cross-sections are depicted in Fig. 5.



The factors  $x_a f_{a/A}$  and  $x_b f_{b/B}$  in (6) give the probability for finding the incoming partons  $a, b$  in the beam particles  $A, B$  with momentum fractions  $x_{a,b}$ . The formfactors  $\mathcal{S}_{a,b}$  are the probabilities for the incoming partons  $a, b$  to emerge directly from the structure functions of  $A, B$  without additional initial state evolution as illustrated in Fig.3 (conversely,  $1 - \mathcal{S}_{a,b}$  determine the amount of real and virtual initial-state radiation). The explicit expression for  $S_a$  (and similarly for  $S_b$ ) reads [23–25],

$$S_a(x_a, \mu^2, Q^2 | t) = \exp \left\{ - \sum_{a'} \int_{-\infty}^t dt' \int d^3 \bar{\mathbf{r}} \int_{\mu^2}^{Q^2} \frac{dk'^2}{k'^2} \int_{z_-}^{z_+} \frac{dz}{z} \frac{\alpha_s((1-z)k'^2)}{2\pi} \gamma_{a' \rightarrow a}(z) \right. \\ \left. \times \left( \frac{f(x_{a'}, k'^2)}{f(x_a, k'^2)} \right) \theta \left( t - t' - \frac{k'_0}{k'^2} \right) \delta^3 \left( \bar{\mathbf{r}} - \frac{\mathbf{k}'}{k'_0} t' \right) \right\}, \quad (11)$$

where the sum runs over the possible species  $a' = g, q, \bar{q}$ , and the function  $\gamma_{a' \rightarrow a}(z)$  with energy fraction  $z = k_{0a}/k_{0a'}$  is the well-known DGLAP kernel [19,20] for the energy distribution in the branching  $a' \rightarrow a$ . The integration limits  $z^+ = 1 - z^- = 1 - k^2/\mu^2$  of the  $z$ -integration arise from the kinematic constraints of the branching  $a \rightarrow a'$ . Last but not least, the final-state evolution of the recoiling parton  $d$  in Fig. 3 is incorporated in the time-like form factor [23–25],

$$T_d(Q^2, \mu^2 | t) = \exp \left\{ - \sum_{d'} \int_t^\infty dt' \int d^3 \bar{\mathbf{r}} \int_{\mu^2}^{Q^2} \frac{dk'^2}{k'^2} \int_{z_-}^{z_+} dz \frac{\alpha_s((1-z)k'^2)}{2\pi} \gamma_{d \rightarrow d'}(z) \right. \\ \left. \times \theta \left( t - t' - \frac{k'_0}{k'^2} \right) \delta^3 \left( \bar{\mathbf{r}} - \frac{\mathbf{k}'}{k'_0} t' \right) \right\}, \quad (12)$$

which is summed over the species  $d' = g, q, \bar{q}$  of the possible daughter species  $d'$ , and the phase-space boundary for the branching is again  $z^+ = 1 - z^- = 1 - \mu^2/k^2$ .

I emphasize that the expressions (11) and (12) are ‘space-time generalizations’ of the standard space-like and time-like form factors with so-called angular ordering derived within the leading-log approximation including coherence effects [20,26]. By integrating over all times  $t \rightarrow \infty$  and over the spatial variables, one would regain the commonly used momentum-space expressions that make no reference to the space-time development of the evolution. Characteristic of the above space-time dependent form factors is the appearance of the  $\theta$ - and  $\delta$ -functions: First, the factor  $\theta(\delta t - k_0/k^2)$  accounts for the mean formation time  $t_{form} = \gamma \tau_{form} = (k_0/k)(1/k)$  of a gluon emission with the energy  $k_0$ . By enforcing that  $t_{form}$  must be smaller than or equal to the considered time interval  $\Delta t = t - t'$ , one ensures that the emitted offspring becomes incoherently separate from radiating mother. Notice that instead of  $\theta(\Delta t - t_{form})$ , one could use a smeared-out distribution such as  $\exp(-\Delta t/t_{form})$ . The results are rather independent of the specific form, provided only that the choice respects the uncertainty principle. Secondly, the factor  $\delta^3(\bar{\mathbf{r}} - \mathbf{v} t')$  with the velocity  $\mathbf{v} = \mathbf{k}/k_0$  simply reflects the classical propagation of each parton in the cascade evolution, i.e. the spatial development is approximated by straight-line trajectories of the partons between branching vertices.

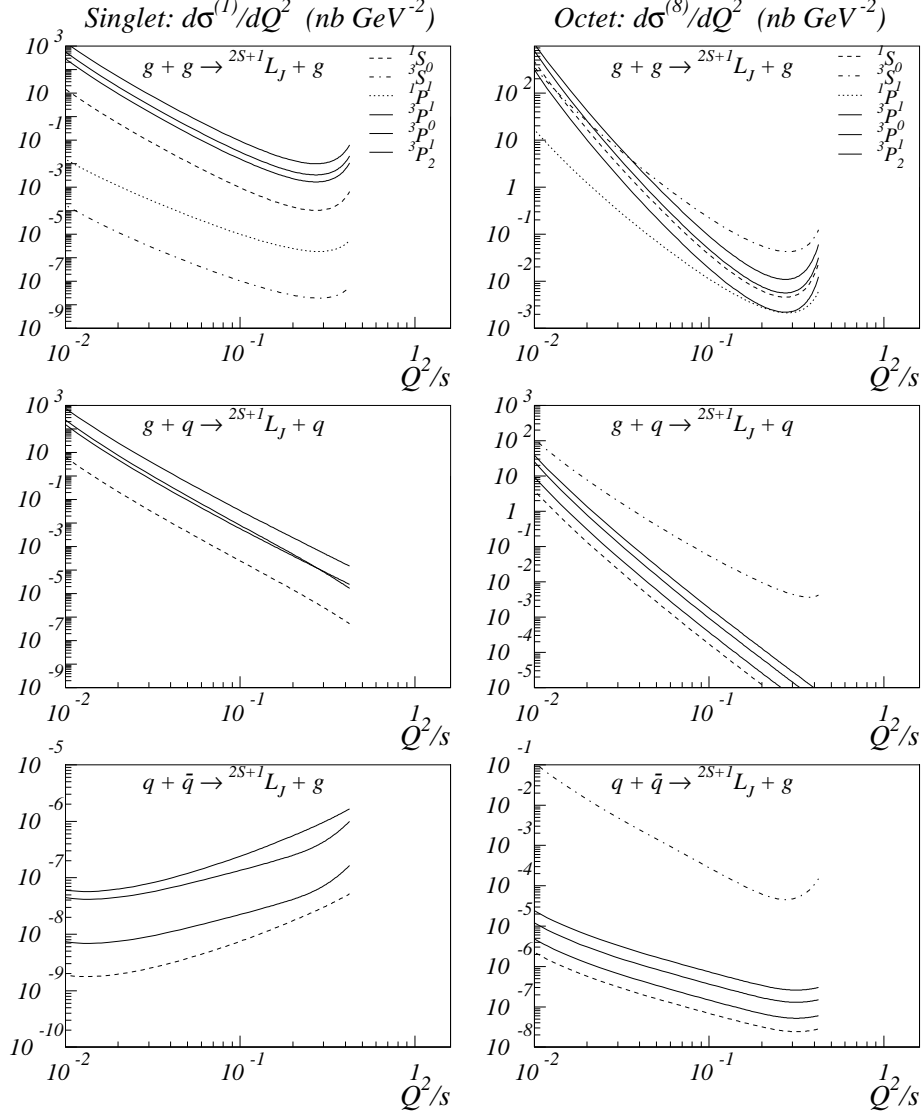


FIG. 4.  $O(\alpha_s^3)$  PQCD cross-sections for the production of  $Q\bar{Q}$  states with specific quantum numbers  $J, L, S$  by a hard parton collisions with energy  $\sqrt{s}$  and momentum transfer  $Q = p_\perp$ , mediated by  $gg, qq$ , and  $q\bar{q}$  collisions. Notice the very different magnitude of color-singlet (left) and color-octet cross-sections (right).

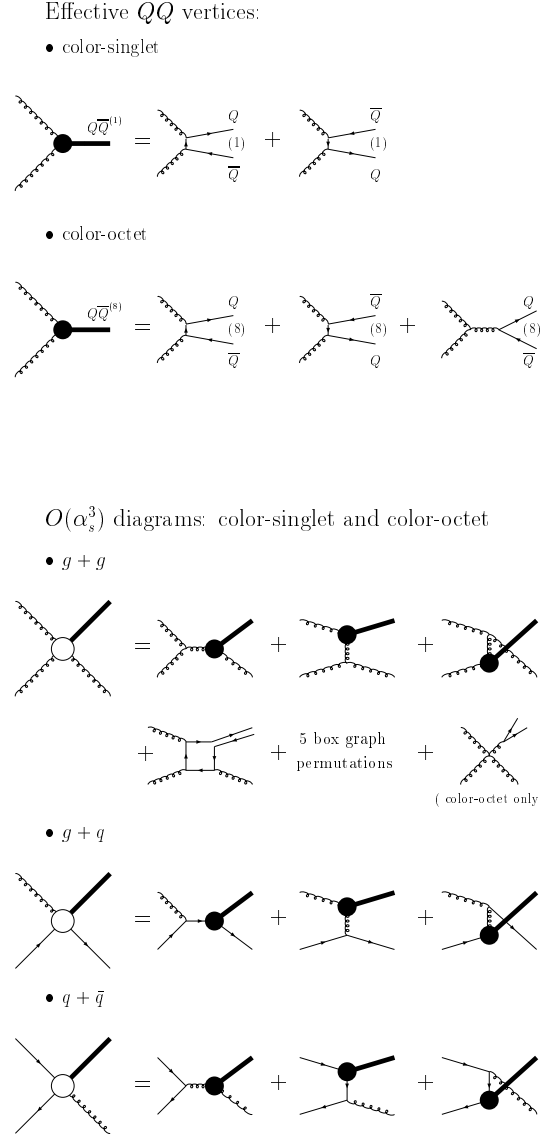


FIG. 5. Color-singlet and color-octet Feynman diagrams that contribute at  $O(\alpha_s^3)$  to  $Q\bar{Q}$  production via the processes (i)  $g + g \rightarrow Q\bar{Q} + g$ , (ii)  $g + q \rightarrow Q\bar{Q} + g$ , and (iii)  $q + \bar{q} \rightarrow Q\bar{Q} + g$ . The top part defines the solid blobs with a fat line attached as effective vertices, which are to be understood as insertions in the diagrams of the lower part.

## B. Evolution

The amplitude  $\mathcal{A}\left(c^* \rightarrow [Q\bar{Q}]^{JLS,(1)} + m g + m' q + \overline{m'} \bar{q}\right)_{\text{evolution}}$  describes the perturbative evolution subsequent to the hard production of the time-like fluctuation  $c^* = Q\bar{Q}$  or  $c^* = g$ . If  $c^* = Q\bar{Q}$  (Fig. 2a, 3a), the  $Q\bar{Q}$  pair is produced directly at the hard vertex, i.e., without intermediate gluon, so that there is only one stage, namely the evolution of the  $Q\bar{Q}$  until it becomes a hadron  $H_{Q\bar{Q}}$ . If  $c^* = g$  (Fig. 2b, 3b), there are two stages involved: first, the evolution of the time-like gluon through real and virtual gluon radiation until it decays into a (off-shell)  $Q\bar{Q}$  pair, and second the analogous evolution of the virtual  $Q\bar{Q}$  until it converts into a bound-state upon hadronization. Both cases can be incorporated by representing  $\mathcal{E}_{c^*}^2$  as follows:

$$\begin{aligned} \mathcal{E}_{c^*}^2(Q^2, \mu^2 | k_1, k_2, \bar{\mathbf{r}}_1, \bar{\mathbf{r}}_2, t) &\equiv \left| \mathcal{A}\left(c^* \rightarrow [Q\bar{Q}]^{JLS,(1)} + m g + m' q + \overline{m'} \bar{q}\right)_{\text{evolution}} \right|^2 \\ &= \int_{t_0}^t \int d^3\bar{\mathbf{r}}_{c^*} \int_{\mu^2}^{Q^2} \frac{dk^2}{k^2} \int dx \int dz \mathcal{F}_{c^*}(x, z, Q^2, k^2 | \bar{\mathbf{r}}_{c^*}, t) \\ &\quad \times \frac{1}{zx} D_Q^Q\left(\frac{x_1}{zx}, k^2, \mu^2 | \bar{\mathbf{r}}_1, t\right) \frac{1}{(1-z)x} D_{\bar{Q}}^{\bar{Q}}\left(\frac{x_2}{(1-z)x}, k^2, \mu^2 | \bar{\mathbf{r}}_2, t\right). \end{aligned} \quad (13)$$

Here the space-time dependent parton densities  $D_a^b(x, k^2, \mu^2 | \bar{\mathbf{r}}, t)$  embody the resummation of the leading-log corrections from virtual and real gluon emissions to all orders in  $\alpha_s$  according to the DGLAP equations [19], that is,

$$D_a^b(x, k^2, \mu^2 | \bar{\mathbf{r}}, t) = \sum_c \int_{t_0}^t dt' \int d^3\bar{\mathbf{r}} \int_{\mu^2}^{k^2} \frac{dk'^2}{k'^2} \int dz \frac{\alpha_s((1-z)k'^2)}{2\pi} \gamma_{a \rightarrow c}(z) \theta\left(t - t' - \frac{k'_0}{k'^2}\right) \delta^3\left(\bar{\mathbf{r}} - \frac{\mathbf{k}'}{k'_0} t'\right), \quad (14)$$

with  $\gamma_{a \rightarrow c}(z)$  again denoting the DGLAP kernel for branching  $a \rightarrow c$ . In (13) the function  $\mathcal{F}_{c^*}$  depends on whether the  $Q\bar{Q}$  pair is produced directly at the hard vertex (fig. 2a, 3a) or via gluon fragmentation (Fig. 2b, 3b):

$$\mathcal{F}_{c^*}(x, z, Q^2, k^2 | \bar{\mathbf{r}}_{c^*}, t) = \begin{cases} \delta(1-x) \delta\left(1 - \frac{k^2}{Q^2}\right) \delta(\bar{\mathbf{r}}_{c^*} - \bar{\mathbf{R}}_0) & \text{if } c^* = Q\bar{Q} \\ D_g^g(x, Q^2, k^2 | \bar{\mathbf{r}}_{c^*}, t) \frac{\alpha_s((1-z)k^2)}{2\pi} \Gamma_{g \rightarrow Q\bar{Q}}(z) & \text{if } c^* = g \end{cases}. \quad (15)$$

On the right side, for the case  $c^* = g$ , the kernel  $\Gamma(z)$  is now the *real* branching probability and not the sum of real and virtual contributions as the above  $\gamma(z)$ , since a *real*  $Q\bar{Q}$  pair has to be produced. The two functions are related, however, by

$$\gamma_{a \rightarrow b}(z) = \Gamma_{a \rightarrow bb'}(z) - \delta_{ab} \delta(z-1) \frac{1}{2} \sum_{c,c'} \int_0^1 dy \Gamma_{a \rightarrow cc'}(y). \quad (16)$$

For the case  $c^* = Q\bar{Q}$ , the product of  $\delta$ -functions simply cause the integrations over the intermediate  $c^*$  to collapse and enforce the  $Q\bar{Q}$  to be produced directly at the mean position  $\bar{\mathbf{R}}$  at the hard vertex at time  $t_0$ .

The *physical interpretation* of eq. (13) in conjunction with (15) is rather evident: the product of the functions  $D$  contain the cumulative effect of the perturbative evolution of the produced  $c^*$  at  $Q^2$  and of the final  $Q\bar{Q}$  pair: either (i) directly, if  $c^* = Q\bar{Q}$ , the evolution of the  $Q\bar{Q}$  from  $Q^2$  to the point when it hadronizes, but at most to the factorization point  $\mu^2$  in (7); or (ii) by fragmentation of the gluon, if  $c^* = g$ , from  $Q^2$  to  $k^2$ , the decay into  $Q\bar{Q}$  at  $k^2$  and the subsequent evolution of the pair from  $k^2$  to  $\mu^2$  (or above  $\mu^2$ , if the  $Q\bar{Q}$  form a bound-state beforehand, in which case the evolution terminates).

## C. Coalescence

The final ingredient in the total amplitude (2), is the subamplitude  $\mathcal{A}\left([Q\bar{Q}]^{JLS,(1)} \rightarrow H_{Q\bar{Q}}^{(2S+1)L_J}\right)_{\text{coalescence}}$  for the conversion of the final state  $Q\bar{Q}$  pair into the bound-state hadron  $H_{Q\bar{Q}}$ . Again, I am interested in the square of this subamplitude,

$$\mathcal{C}_{JLS}^2(\mu^2 | k_1, k_2, \bar{\mathbf{r}}_1, \bar{\mathbf{r}}_2, t) \equiv \left| \mathcal{A} \left( [Q\bar{Q}]^{JLS,(1)} \rightarrow H_{Q\bar{Q}}^{(2S+1)L_J} \right)_{\text{coalescence}} \right|^2. \quad (17)$$

Clearly, in view of the unknown details of the non-perturbative physics, the coalescence of  $Q\bar{Q}$  to a bound-state and eventually to a physical quarkonium state, requires some model input, and therefore introduces a model dependence contrary to the previous elements of the PQCD description of production and evolution. The rationale is here, to avoid the introduction of free parameters and develop a transparent and practical bound-state formalism within the principles of NRQCD.

### 1. Scheme of approximation

Starting from the amplitude level, the ‘unsquared’  $\mathcal{C}$  can be expressed in the usual fashion of time-dependent perturbation theory on the basis of the Dyson series [27],

$$\begin{aligned} \mathcal{C}_{JLS}(\mu^2 | k_1, k_2, \bar{\mathbf{r}}_1, \bar{\mathbf{r}}_2, t) &= -i \int_{t_0}^t dt' \langle \Psi | V(\mu^2, \bar{\mathbf{R}}, t') | [\psi \bar{\psi}] \rangle \\ &= \langle \Psi | \tilde{V}(\mu^2, \bar{\mathbf{R}}) | [\psi \bar{\psi}] \rangle (1 - e^{i\Delta E t}), \end{aligned} \quad (18)$$

where  $\Delta E = E_{Q\bar{Q}} - E_H$ , the wave-functions of the  $Q$  and  $\bar{Q}$  are denoted by  $\psi, \bar{\psi}$  (the brackets [...] indicating the  $Q\bar{Q}$  coupling to a color-singlet and specific total spin state as described below), and  $\Psi$  is the bound-state wave-function of  $H_{Q\bar{Q}}$ . The transition operator

$$V(\mu^2, \bar{\mathbf{R}}, t) = \tilde{V}(\mu^2, \bar{\mathbf{R}}) e^{i\Delta E t} \quad (19)$$

represents the non-perturbative mechanism of conversion from the partonic  $Q\bar{Q}$  state to the hadronic bound-state  $H_{Q\bar{Q}}$ , which in principle may depend on time  $t$ , the center-of-mass position  $\bar{\mathbf{R}}$ , and of course on the factorization scale  $\mu^2$ . Unfortunately the non-perturbative operator  $V$  cannot be inferred from first principles at present, so that one is forced to rely on lattice results, or phenomenological model building. Most previous quarkonium studies simply treated the unknown non-perturbative amplitude in (17) or (18) as a parameter, i.e., a number being determined either from fits to experimental data or taken from NRQCD potential models.

Instead, I follow a different approach and try to actually *calculate* approximately this amplitude on the basis of the following arguments: It is well known from hadronization studies of jet fragmentation that the mechanism of parton-hadron conversion at high energies appears to be a universal and local phenomenon [28,29], in the sense that it is rather independent of the space-time history of the hadronizing partons and essentially determined by the final-state configuration of neighboring partons in a local phase-space cell. Moreover it is known that the actual details of the hadronization dynamics are irrelevant for simple observables as hadron production rates. Hence, it is near at hand to assume that the operator  $V$ , eq. (19), is approximately of local nature, in the sense that its time variation is sufficiently slow that it may be omitted with respect to the  $Q\bar{Q}$  motion, and furthermore is at best weakly dependent on  $\bar{\mathbf{R}}$  (which in the presence of translational invariance is certainly the case). Accordingly, I make the following key approximation, pulling  $\tilde{V}$  out of the matrix-element (18):

$$\langle \Psi | \tilde{V}(\mu^2, \bar{\mathbf{R}}) | [\psi \bar{\psi}] \rangle \longrightarrow \langle \tilde{V} \rangle \times \langle \Psi | [\psi \bar{\psi}] \rangle. \quad (20)$$

Returning to (18), I insert (20), take the square, and integrate over the hadronic energy spectrum  $dE_H$  weighted with the level density  $\rho(E_h)$ , and obtain so the approximate result for the squared amplitude  $\mathcal{C}^2$  of eq. (17):

$$\begin{aligned} \mathcal{C}_{JLS}^2(\mu^2 | k_1, k_2, \bar{\mathbf{r}}_1, \bar{\mathbf{r}}_2, t) &\approx \int_{\mu} dE_H \rho(E_H) \left| \langle \tilde{V} \rangle \right|^2 \frac{4}{(\Delta E)^2} \sin^2 \left( \frac{\Delta E t}{2} \right) |\langle \Psi | [\psi \bar{\psi}] \rangle|^2 \\ &\stackrel{t \rightarrow \infty}{\equiv} 2\pi t \rho(E_H) \left| \langle \tilde{V} \rangle \right|^2 |\langle \Psi | [\psi \bar{\psi}] \rangle|^2 \\ &\simeq |\langle \Psi | [\psi \bar{\psi}] \rangle|^2, \end{aligned} \quad (21)$$

Here I have in the second step exploited the fact that only those final states contribute significantly for which  $t \sim 2\pi/\Delta E$ , i.e.,  $\Delta t \Delta E \sim 1$  with  $\Delta t = t - t_0$ , and in the last step I have assumed that the energy spectrum  $\rho(E_H) \propto 1/E_H$ , which is roughly satisfied by the known hadron states. Because the time scale  $\Delta t$  for the conversion from  $Q\bar{Q}$  to  $H_{Q\bar{Q}}$  is related by the uncertainty principle to the energy difference  $\Delta E$  between the quarkonic and hadronic states, the approximation (20) and (21) reduces the unknown matrix-element (17) to the simple overlap matrixelement between the heavy quark pair  $Q\bar{Q}$  and the bound-state hadron  $H_{Q\bar{Q}}$ .

## 2. Wave-functions

To proceed from (21), the goal is to model the non-perturbative dynamics of conversion of the final  $Q$  and  $\bar{Q}$  into the bound-state hadron  $H_{Q\bar{Q}}$  by making a specific ansatz for the wave-functions  $\Psi$  and  $\psi, \bar{\psi}$ . I shall adopt the well-established NRQCD bound-state picture for quarkonia [7] in conjunction with coalescence framework developed in Refs. [21]. As proclaimed before, I restrict the considerations to  $S$ -wave and  $P$ -wave bound-states with angular momentum  $L = 0$  and  $L = 1$ , respectively. The corresponding bound-state wave-functions are therefore of scalar, respectively vector character in angular momentum space. In the quarkonium bound-state formalism, developed in detail in Ref. [7], the bound-state wave-function is constructed in terms of the overlap amplitude between quark and antiquark spinors  $\psi$  and  $\bar{\psi}$  in a given total spin configuration (singlet  $S = 0$  or triplet  $S = 1$ ) and the bound-state wave-function  $\Psi$  in a given angular momentum state  $L = 0$  or  $L = 1$ , to form a state of total angular momentum  $J = 0, 1, 2$ . As usual, I assume that in the restframe of the bound-state the relative momentum  $|\mathbf{k}| = \frac{1}{2}|\mathbf{k}_1 - \mathbf{k}_2|$  of the  $Q$  and  $\bar{Q}$  with 3-momenta  $\mathbf{k}_1$  and  $\mathbf{k}_2$ , respectively, is small as compared to the quark mass  $M_Q$ . As a consequence, one can decompose the (unsquared) amplitude  $\mathcal{C}_{JLS}$ , eq. (21), in coordinate space as follows:

$$\mathcal{C}_{JLS}(\mu^2 | k_1, k_2, \bar{\mathbf{r}}_1, \bar{\mathbf{r}}_2, t) = 2\pi\delta\left(t - \frac{t_1 + t_2}{2}\right) \frac{1}{\sqrt{2J+1}} \sum_{M, S_z} \langle L M, S S_z | J J_z \rangle \Psi_M^{L*}(\mathbf{r}_1, \mathbf{r}_2) [\psi \bar{\psi}]_{S_z}^{S(1)}(\mathbf{r}_1, \mathbf{r}_2). \quad (22)$$

Here  $\langle L M, S S_z | J J_z \rangle$  is the Clebsch-Gordan coefficient for the coupling of spin  $S$  and relative angular momentum  $L$  to a total  $J$  with associated projections  $S_z, M$ , and  $J_z$ , respectively,  $\Psi_M^{L*}$  is the complex conjugate of the bound-state wave-function for a  $L$ -state with projection  $M$ , and

$$[\psi \bar{\psi}]_{S_z}^{S(1)}(\mathbf{r}_1, k_1; \mathbf{r}_2, k_2) = \frac{1}{\sqrt{2N_c}} \sum_{c_1, c_2=1}^{N_c} \langle 3i, \bar{3}j | 10 \rangle \sum_{s_1, s_2} \langle \frac{1}{2} s_1, \frac{1}{2} s_2 | S S_z \rangle \psi(\mathbf{r}_1, s_1, c_1) \bar{\psi}(\mathbf{r}_2, s_2, c_2) \quad (23)$$

ouples the  $Q$  and  $\bar{Q}$  spinors to a color-singlet with total spin  $S$  and projection  $S_z$ .

To proceed, one needs to specify the wave-functions  $\Psi$  and  $\psi, \bar{\psi}$ . Most plausible would be to use quarkonium wave functions from potential model calculations, which however are not available analytic form. Therefore, I choose instead to work with harmonic oscillator wave-functions for which it is possible to obtain the overlap integrals involving  $\Psi, \psi, \bar{\psi}$ , as transparent, closed expressions. Following the coalescence approach of Refs. [21], I shall assume that quark  $Q$  and antiquark  $\bar{Q}$  may be described by wave-packets of width  $\sigma_i \propto 1/\sqrt{k_i^2}$  ( $k_i^2 = k_{0i}^2 - \mathbf{k}_i^2$ ), localized in space around  $\bar{\mathbf{r}}_i$  and in momentum space around  $\bar{\mathbf{k}}_i$ , multiplied by the usual  $SU(2)$  and  $SU(3)$  spinors  $\chi, \xi$  for spin and color, respectively:

$$\psi(\mathbf{r}_i, s_i, c_i) = \frac{1}{(\pi \sigma_i^2)^{3/4}} \exp\left(-\frac{(\mathbf{r}_i - \bar{\mathbf{r}}_i)^2}{2\sigma_i^2}\right) \exp(i\bar{\mathbf{k}}_i \cdot \mathbf{r}_i) \chi_{s_i}^{\frac{1}{2}} \xi_{c_i}^{\frac{1}{3}} \quad i = 1, 2 \quad (= Q, \bar{Q}) \quad (24)$$

Here and in the following the notation of 3-vectors is such that, e.g.,  $\bar{\mathbf{r}}_i$  refers to the mean position as a classical variable, whereas  $\mathbf{r}_i$  describes the quantum-mechanical fluctuation of a particle's position around the mean value. Notice that the plane-wave factor  $\exp(i\bar{\mathbf{k}}_i \cdot \mathbf{r}_i)$  ensures the uncertainty principle in the sense that a classical particle interpretation is only possible if  $|\mathbf{r}| \ll 1/|\bar{\mathbf{k}}_i|$ .

The bound-state wave function  $\Psi$  on the other hand, I write as a product of its center-of-mass motion and its internal motion, again in terms of Gaussian wave-packets, the size of which generally depends on the particular orbital angular momentum state, and of course on the flavor of the heavy-quark pair. Defining center-of-mass and relative coordinates and momenta as

$$\begin{aligned} \mathbf{R} &= \frac{\mathbf{r}_1 + \mathbf{r}_2}{2} & \mathbf{r} &= \mathbf{r}_1 - \mathbf{r}_2 \\ \mathbf{K} &= \mathbf{k}_1 + \mathbf{k}_2 & \mathbf{k} &= \frac{\mathbf{k}_1 - \mathbf{k}_2}{2}, \end{aligned} \quad (25)$$

and similarly for the mean positions  $\bar{\mathbf{R}}, \bar{\mathbf{r}}$  and momenta  $\bar{\mathbf{K}}, \bar{\mathbf{k}}$ , I make the factorized ansatz

$$\Psi_M^L(\mathbf{r}_1, \mathbf{r}_2) = \Phi^L(\mathbf{R}) \phi_M^L(\mathbf{r}). \quad (26)$$

The center-of-mass wave-function  $\Phi^L$  depends on  $L$  in its spatial width,

$$\Phi^L(\mathbf{R}) = \frac{1}{(\pi \Sigma_L^2)^{3/4}} \exp\left(-\frac{(\mathbf{R} - \bar{\mathbf{R}})^2}{2\Sigma_L^2}\right) \exp(i\bar{\mathbf{K}} \cdot \mathbf{R}) \quad (27)$$

and the relative motion  $\phi_M^L$  depends on both  $L$  and its projection  $M$ ,

$$\phi_M^L(\mathbf{r}) = \frac{\mathcal{N}_L}{(\pi \alpha_L^2)^{3/4}} r^L \exp\left(-\frac{r^2}{2\alpha_L^2}\right) Y_{LM}(\hat{\mathbf{r}}), \quad (28)$$

with the  $L$ -dependent prefactors  $\mathcal{N}_0 = 1$  and  $\mathcal{N}_1 = \sqrt{2/3}$  and the spherical harmonics  $Y_{LM}$  depending on the angular orientation  $\hat{\mathbf{r}} = \mathbf{r}/r$ , where  $r \equiv |\mathbf{r}|$ .

### 3. Coalescence probabilities

Inserting the wave-functions  $\psi, \bar{\psi}$  and  $\Psi$  into (23), integrating over  $\mathbf{r}_1 = \mathbf{R} + \frac{1}{2}\mathbf{r}$  and  $\mathbf{r}_2 = \mathbf{R} - \frac{1}{2}\mathbf{r}$ , summing over the angular momentum projections, and then squaring the resulting amplitude  $\mathcal{C}_{JLS}$ , one obtains the *coalescence probability*  $\mathcal{C}_{JLS}^2$  for the conversion of  $Q\bar{Q}$  into bound-states  $^{2S+1}L_J$ . Specifically for the  $S$ - and  $P$ -wave states, one obtains the following closed expressions:

- $S$ -states ( $L = 0, J = S = 0, 1$ ):

$$\mathcal{C}_{J0S}^2(\mu^2 | \bar{k}^2, \bar{r}^2, t) = \left(\frac{1}{4\pi}\right) \left(\frac{4\nu_0}{\sqrt{2}\mu_0}\right)^3 \exp\left(-\frac{\nu_0^2}{2} \bar{k}^2\right) \exp\left(-\frac{1}{\mu_0^2} \bar{r}^2\right) \quad (29)$$

- $P$ -states ( $L = 1, J = L + S = 0, 1, 2$ ):

$$\mathcal{C}_{J1S}^2(\mu^2 | \bar{k}^2, \bar{r}^2, t) = \left(\frac{3}{4\pi}\right) \left(\frac{4\nu_1}{\sqrt{2}\mu_1}\right)^3 \frac{1}{6} \left(\frac{\alpha_1^4}{\mu_1^4} \bar{r}^2 + \nu_1^4 \bar{k}^2\right) \exp\left(-\frac{\nu_1^2}{2} \bar{k}^2\right) \exp\left(-\frac{1}{\mu_1^2} \bar{r}^2\right), \quad (30)$$

In the above formulae (29) and (30) I used  $\bar{k} = |\bar{\mathbf{k}}| = \frac{1}{2}|\bar{\mathbf{k}}_1 - \bar{\mathbf{k}}_2|$ ,  $\bar{r} = |\bar{\mathbf{r}}| = |\bar{\mathbf{r}}_1 - \bar{\mathbf{r}}_2|$ , and

$$\mu_L^2 \equiv 2\sigma^2 + \alpha_L^2 \quad \nu_L^2 \equiv \frac{\sigma^2 \alpha_L^2}{\mu_L^2}. \quad (31)$$

Furthermore,  $\sigma^2 = \frac{1}{2}(\sigma_1^2 + \sigma_2^2)$ , and  $\Sigma_L^2 = \sigma^2/2$ , assuming that the 2-body center-of-mass motion of  $Q$  and  $\bar{Q}$  is unaltered during the coalescence process.

It is worth noting that the final expressions for the coalescence probabilities  $\mathcal{C}_{JLS}^2$  in (29) and (30) are functions of the relative  $Q\bar{Q}$  momentum and separation only, and do not depend neither on the individual variables  $\bar{\mathbf{k}}_i$  and  $\bar{\mathbf{r}}_i$ , nor on the total momentum  $\bar{\mathbf{K}}$  or the *cm*-position  $\bar{\mathbf{R}}$  of the pair. This makes the coalescence process a *local* mechanism, in accordance with the aforementioned locality of hadronization in high-energy particle collisions. Also notice that the coalescence probabilities are time-dependent, although not explicit in (29) and (30), due to the dynamically changing  $Q$  and  $\bar{Q}$  momenta and trajectories, i.e.,  $\bar{k} = \bar{k}(t)$  and  $\bar{r} = \bar{r}(t)$ . Finally, the dependence on  $\mu^2$  indicated by the first argument of  $\mathcal{C}_{JLS}^2$ , is again implicit in the  $Q$  and  $\bar{Q}$  momenta, since per definition  $\mu^2$  serves as a cut-off for soft gluon radiation with energies below  $\mu$  from  $Q$  or  $\bar{Q}$  and hence limits the radiative energy loss of the pair. This in turn influences the coalescence to a  $Q\bar{Q}$  bound-state, although this dependence is very weak.

The independent *parameters* involved in (29) and (30) are  $\sigma^2$  (a property of the  $Q$  and  $\bar{Q}$  upon coalescence, but independent of the bound-states  $H_{Q\bar{Q}}$ ), and  $\alpha_L^2$  (a property of the bound-states  $H_{Q\bar{Q}}$ , depending on the angular momentum quantum number  $L$  as well as on the ‘flavor’,  $c\bar{c}$  or  $b\bar{b}$ ). However, these parameters  $\sigma^2$  and  $\alpha_L^2$  are *not for free choice*. Rather than that, the possible values of  $\sigma^2$ , are given by the invariant (off-shell) masses  $k_i^2 = k_{0i}^2 - \mathbf{k}_i^2$ , and hence are dictated by the dynamics of  $Q$  and  $\bar{Q}$  itself, whereas  $\alpha_L^2$  is determined by the Bohr radii of the various quarkonium states  $H_{Q\bar{Q}}(^{2S+1}L_J)$ . Specifically, for  $\sigma^2 = \frac{1}{2}(\sigma_1^2 + \sigma_2^2)$ , the widths  $\sigma_i$  of the  $Q$  and  $\bar{Q}$  wave-packets are obtained from relating their (time-evolving) invariant masses  $k_i^2$  by means of the uncertainty principle to the corresponding mean spatial sizes <sup>†</sup>,

---

<sup>†</sup> The factors 2/3 in (32) and (33) arise from the definition of the mean square radii of the heavy quarks and the bound-state, respectively, which involve the ratios  $\langle r^2 \rangle = \int d^3r' r'^2 f(r') / \int d^3r' f(r')$ , where  $f(r)$  stands for the Gaussian wave-packets of  $Q$ ,  $\bar{Q}$  and of the bound-state.

$$\sigma_i^2 = \frac{2}{3k_i^2}, \quad k_i^2 = k_{0i}^2 - \mathbf{k}_i^2 \geq M_Q^2, \quad (32)$$

whereas the widths  $\alpha_L$  of the bound-state wave-functions are related to the sizes of the corresponding quarkonium hadrons  $H_{Q\bar{Q}}(^{2S+1}L_J)$  through the measurable electron scattering radii,

$$\alpha_L^2 \equiv \alpha_L^2(H_{Q\bar{Q}}) = \frac{2}{3} R_{Q\bar{Q}}^2, \quad R_{Q\bar{Q}} \equiv R_{Q\bar{Q}}(^{2S+1}L_J). \quad (33)$$

The relevant values of  $R_{Q\bar{Q}}$  for charmonium and bottomonium states that are used later, are listed in Table 1.

	$R_{Q\bar{Q}}(^{2S+1}L_J)$ (fm)					
	$^1S_0$	$^3S_1$	$^1P_1$	$^3P_0$	$^3P_1$	$^3P_2$
$c\bar{c}$	$\eta_c$	$J/\psi$	$h_c$	$\chi_{c0}$	$\chi_{c1}$	$\chi_{c2}$
	0.25	0.27	0.55	0.60	0.63	0.66
$b\bar{b}$	$\eta_b$	$\Upsilon$	$h_b$	$\chi_{b0}$	$\chi_{b1}$	$\chi_{b2}$
	0.10	0.12	0.25	0.29	0.31	0.33

TABLE I. Quarkonium RMS values  $R_{Q\bar{Q}}$  used for the widths of bound-state wave functions with different  $J, L, S$  in conjunction with the relation (33).

The coalescence probabilities (29) and (30) consist (apart from the normalization factors that are always  $\leq 1$ ) of two Gaussians, one in momentum space,  $\exp(-\nu^2 \bar{k}^2/2)$ , and one in position space,  $\exp(-\bar{r}^2/\mu^2)$ . The first one ensures the conservation of momentum, whereas the second restricts the distance between the coalescing  $Q$  and  $\bar{Q}$  to a width which is given by the bound-state size, augmented by the uncertainty in the positions of the  $Q$  and  $\bar{Q}$ . The essential difference between the  $S$ -wave coalescence probabilities (29) and the  $P$ -wave counterpart (30), is the factor  $(\alpha^4 \bar{r}^2/\mu^4 + \nu^4 \bar{k}^2)$  present in the latter. For  $\bar{\mathbf{k}} \rightarrow 0$  the  $P$ -wave probability  $\mathcal{C}_{J1S}^2$  therefore vanishes, reaches a maximum as  $\bar{\mathbf{r}}$  increases, and then tends to zero again with an exponential tail. Contrary to this, the  $S$ -wave probability  $\mathcal{C}_{J0S}^2$ , for  $\bar{\mathbf{k}} \rightarrow 0$ , has a maximum at  $\bar{\mathbf{r}} = 0$  and damps out exponentially as  $\bar{\mathbf{r}}$  increases. This characteristic behavior is plotted in Fig. 6, which shows the coalescence probabilities (29) and (30) for the different angular momentum eigenstates  $^{2S+1}L_J$  as a function of  $\bar{r} \equiv |\bar{\mathbf{r}}|$  for various values of  $\bar{k} \equiv |\bar{\mathbf{k}}|$ .

#### 4. Relation between $\mathcal{C}_{JLS}$ and commonly used quarkonium wave-functions $\mathcal{R}_L(0)$

At this point, it is instructive to relate the coalescence probabilities  $\mathcal{C}_{JLS}^2$  in (29) and (30) with their analogues in earlier quarkonium studies, namely the values of the squared radial quarkonium wave-functions at the origin,  $|\mathcal{R}_L(0)|^2$ , where

$$\mathcal{R}_L(0) \equiv \left. \frac{\partial^L}{\partial r^L} \mathcal{R}_L(r) \right|_{r=0}, \quad (34)$$

with  $r \equiv |\mathbf{r}|$ . Interrelating  $|\mathcal{R}_L(0)|^2$  and  $\mathcal{C}_{JLS}^2$  is somewhat ambiguous, because the latter coalescence probabilities are to be weighted with and summed over all possible  $Q\bar{Q}$  configurations with distinct relative momentum and spatial separation, while the former  $|\mathcal{R}_L(0)|^2$  is just a number, independent of space-time and the momentum distribution of  $Q$  and  $\bar{Q}$ . Hence, one expects the summed-over coalescence probabilities generally be larger. Nevertheless, one may establish as a limiting estimate an approximate correspondence between the  $\mathcal{C}_{JLS}^2$  and the  $|\mathcal{R}_L(0)|^2$  by concentrating on the phase-space region where coalescence receives its dominant contribution from, namely at the maximum value. This is in accord with the commonly used approximation of using the value of is approximately given by  $\mathcal{R}_L(r)$  at  $r = 0$  where the radial wave-function is maximal.



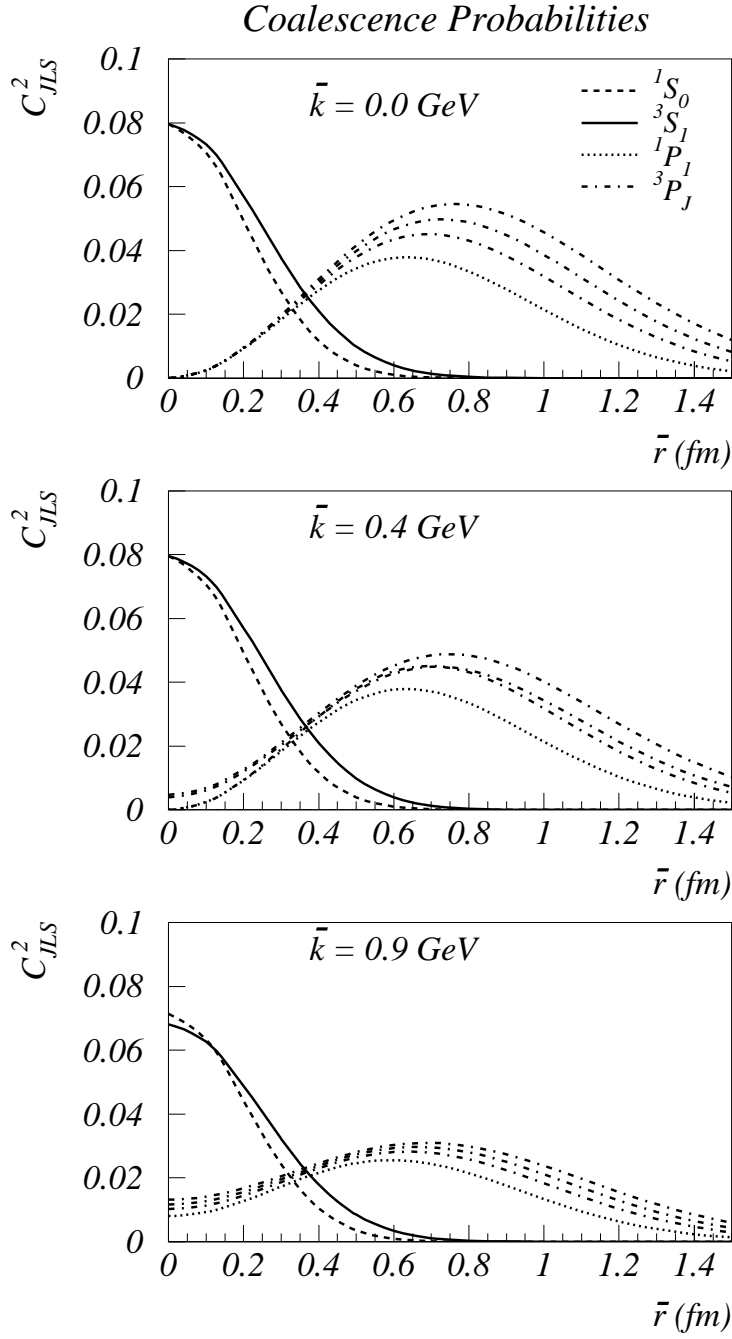


FIG. 6. Typical shape of the coalescence probabilities (29) and (30) for the different angular momentum eigenstates  $^{2S+1}L_J$  as a function of  $\bar{r} \equiv |\bar{\mathbf{r}}|$  for various values of  $\bar{k} \equiv |\bar{\mathbf{k}}|$ . The values of  $\mu_L$  and  $\alpha_L$  entering the expressions (29) and (30) are determined from (31) and (33), using the RMS values of Table 1.

Consequently, one may write

$$\mathcal{C}_{JLS}^2 \left( \mu^2 | \bar{k}^2, \bar{r}_{max}^2(L), t_c \right) \hat{=} \frac{3}{4\pi (M_Q)^{2L}} \int_{R_{Q\bar{Q}}} d^3r |\mathcal{R}_L(0)|^2 \left( 1 + O(\bar{k}^2) \right), \quad (35)$$

where the maximum values of the coalescence probabilities (29) and (30) are

$$\bar{r}_{max}^2(L) = \begin{cases} 0 & \text{for } L = 0 \\ \alpha_L & \text{for } L = 1 \end{cases}, \quad (36)$$

and  $t = t_c$  is the corresponding time argument that can be set to zero, since it is a dummy variable for the present exercise. The integration is over the typical bound-state size with radius  $R_{Q\bar{Q}} \equiv R_{Q\bar{Q}}(^{2S+1}L_J)$ . In the limit  $\bar{k}^2 \rightarrow 0$  one may therefore write for the cases  $L = 0$  and  $L = 1$ , respectively,

$$\mathcal{C}_{J0S}^2(\mu^2|0,0,0) \stackrel{(k \rightarrow 0)}{\approx} |\mathcal{R}_0(0)|^2 R_{Q\bar{Q}}^3, \quad \mathcal{C}_{J1S}^2(\mu^2|0,\alpha_1,0) \stackrel{(k \rightarrow 0)}{\approx} \frac{M_Q^2}{|\mathcal{R}_1(0)|^2} R_{Q\bar{Q}}^3 \quad \text{for } L=2. \quad (37)$$

Typical values for  $|\mathcal{R}_L(0)|^2$  from QCD potential model calculations [30], e.g. for Buchmüller-type wave-functions, are

$$|\mathcal{R}_0(0)|^2 = \begin{cases} 0.81 \text{ GeV}^3 & \text{for } c\bar{c} \\ 6.48 \text{ GeV}^3 & \text{for } b\bar{b} \end{cases} \quad \frac{|\mathcal{R}_1(0)|^2}{M_Q^2} = \begin{cases} 0.041 \text{ GeV}^3 & \text{for } c\bar{c} \\ 0.057 \text{ GeV}^3 & \text{for } b\bar{b} \end{cases} \quad (38)$$

for  $S$ -wave and  $P$ -wave states, respectively, with  $M_c = 1.35 \text{ GeV}$  and  $M_b = 5 \text{ GeV}$ . Comparing these values with the coalescence probabilities in the limit (37), one obtains, on account of the explicit expressions (29) and (30), and using the values of  $R_{Q\bar{Q}}^{(2S+1)L_J}$  from Table 1, the following estimates for  $S$ -states and  $P$ -states, respectively:

$$\frac{1}{R_{Q\bar{Q}}^3} \frac{\mathcal{C}_{J0S}^2(\mu^2|0,0,0)}{|\mathcal{R}_0(0)|^2} \simeq \begin{cases} 1.23 & \text{for } c\bar{c} \\ 1.29 & \text{for } b\bar{b} \end{cases}, \quad \frac{M_Q^2}{R_{Q\bar{Q}}^3} \frac{\mathcal{C}_{J1S}^2(\mu^2|0,\alpha_1,0)}{|\mathcal{R}_1(0)|^2} \simeq \begin{cases} 1.15 & \text{for } c\bar{c} \\ 1.30 & \text{for } b\bar{b} \end{cases}. \quad (39)$$

One sees that these ratios for  $S$ -wave and  $P$ -wave states, respectively, indicate that the coalescence model used in this paper gives around 15-30 % larger values for the formation probabilities of quarkonium than the widely used approximation based on the values of the radial wave-functions at zero  $Q\bar{Q}$  separation. It has to be kept in mind, though, that the actual magnitude of the coalescence probabilities can be significantly larger than in (39) when summed over all possible  $Q\bar{Q}$  momentum configurations and trajectories.

#### D. Cross-sections

In order to make contact with observable quantities such as multiplicities, relative abundances or spectra of produced quarkonium mesons, one needs to integrate the space-time dependent total squared amplitude (3) over the complete event history of a collision  $A+B$ , as well as over all unobserved particle states  $X$ . For instance, the total production cross-section for quarkonia  $H_{Q\bar{Q}}^{(2S+1)L_J}$  is obtained after dividing by the incoming parton flux and setting without loss of generality  $t_0 = 0$ ,  $\bar{\mathbf{R}}_0 = \mathbf{0}$ ,

$$d\sigma(AB \rightarrow H_{Q\bar{Q}} + X) = \sum_{c^*=g, Q\bar{Q}} d\sigma(AB \rightarrow c^* X)(\hat{s}, Q^2) \times \Omega_{c^*}^{JLS}(Q^2, \mu^2), \quad (40)$$

where

$$\begin{aligned} d\sigma(AB \rightarrow c^* X)(\hat{s}, Q^2) &= \sum_{abd} f_{a/A}(x_a, \mu^2) f_{b/B}(x_b, \mu^2) S_a(x_a, \mu^2, Q^2|0) S_b(x_b, \mu^2, Q^2|0) T_d(Q^2, \mu^2|0) \times \\ &\times \left( \frac{1}{2\hat{s}} |A(ab \rightarrow c^* d)|^2(\hat{s}, Q^2) \right) (2\pi)^4 \delta(k_a + k_b - k_{c^*} - k_d) dx_a dx_b d^4 k_{c^*} d^4 k_d. \end{aligned} \quad (41)$$

and

$$\Omega_{c^*}^{JLS}(Q^2, \mu^2) = \int_0^\infty dt \int d^3 \bar{\mathbf{r}}_1 d^3 \bar{\mathbf{r}}_2 \int d^4 k_1 d^4 k_2 \mathcal{E}_{c^*}^2(Q^2, \mu^2|k_1, k_2, \bar{\mathbf{r}}_1, \bar{\mathbf{r}}_2, t) \mathcal{C}_{JLS}^2(\mu^2|k_1, k_2, \bar{\mathbf{r}}_1, \bar{\mathbf{r}}_2, t). \quad (42)$$

Using the kinematic variable definitions (7)-(10), one can express the triple-differential hadronic cross-section for  $H_{Q\bar{Q}}$  production in terms of the rapidities  $y_1$  of the jet  $c^*$  that initiates the  $Q\bar{Q}$  evolution, the rapidity  $y_2$  of the recoiling jet  $d$  which evolves and fragments by itself, and the common relative transverse momentum  $Q = p_\perp$  possessed by each of the two outgoing jets  $c^*$  and  $d$ ,

$$\frac{d\sigma}{dy_1 dy_2 dp_\perp^2}(AB \rightarrow H_{Q\bar{Q}} + X) = \sum_{c^*=g, Q\bar{Q}} \frac{d\sigma}{dy_1 dy_2 dp_\perp^2}(AB \rightarrow c^* X) \times \Omega_{c^*}^{JLS}(p_\perp^2, \mu^2), \quad (43)$$

where  $\Omega_{c^*}^{JLS}$  is the same as above, and

$$\begin{aligned} \frac{d\sigma}{dy_1 dy_2 dp_\perp^2}(AB \rightarrow c^* X) &= \sum_{abd} x_a f_{a/A}(x_a, \mu^2) x_b f_{b/B}(x_b, \mu^2) \left( \frac{1}{16\pi\hat{s}^2} |A(ab \rightarrow c^* d)|^2(\hat{s}, p_\perp^2) \right) \times \\ &\times S_a(x_a, \mu^2, p_\perp^2|0) S_b(x_b, \mu^2, p_\perp^2|0) T_d(p_\perp^2, \mu^2|0). \end{aligned} \quad (44)$$

## E. Calculation scheme

Due to its probabilistic character, the above formalism is suitable for implementation in a Monte Carlo simulation using the computer program VNI [23], which allows one to trace the microscopic history of the dynamically-evolving particle system in space-time *and* momentum space, from the instant of collision of the beam particles  $A$  and  $B$  to the eventual emergence of quarkonium states plus all other final-state particles. Specifically, following the space-time development of the complete system of particles in a collision event, embodies the dynamics of the  $Q\bar{Q}$  system within the rest of the event, consisting of all other produced partons and the hadronization products, as well as the fragmentation of the spectator partons of the beam remnants of the original  $A$  and  $B$ . This allows to account not only for the correlations of particles in space, time, color and flavor, but also for the statistical occurrence of quarkonium formation by  $Q\bar{Q}$  coalescence versus open charm/bottom production by recombination of  $Q$  and  $\bar{Q}$  with partons of the rest of the event.

Referring for technical details to Ref. [23], I confine myself here to a brief outline of the simulation scheme. The time development in position and momentum space of the space-time dependent admixture of partons and emerging hadronic excitations, including  $Q$  and  $\bar{Q}$  and its final hadronic products, is obtained by following each individual particle through its history with the various probabilities and time scales of interactions sampled stochastically from the relevant cross-sections. The detailed history of the system can thus be traced by evolving the phase-space distributions of particles are evolved in small time steps ( $\Delta t \simeq 10^{-3} \text{ fm}$ ) and 7-dimensional phase-space  $d^3r d^3k dE$ , from the instant of collision between the beam particles  $A$  and  $B$ , all the way until stable final-state hadrons and other particles are left as freely-streaming particles. At any time during the evolution, the state of the  $Q\bar{Q}$  system can be extracted, and so the final quarkonium yield at the end of a collisions event. For the case of  $pp$  and  $p\bar{p}$  collisions on which I shall concentrate in the following, the essential ingredients in this Monte-Carlo procedure are summarized as follows [23]:

- (i) The *initial state* is constructed by decomposing the incoming beam particles,  $p$  and  $\bar{p}$ , into their parton substructure according to measured structure functions <sup>‡</sup> with a spatial distribution given by the Fourier transform of the proton elastic form-factor. The so-initialized phase-space densities of (off-shell) partons are then boosted with the proper Lorentz factor to the center-of-mass frame of the colliding beam particles.
- (ii) The *initial  $Q\bar{Q}$  production* is obtained by triggering on those hard parton collisions  $ab \rightarrow c^*d$  that contain a  $c^* = Q\bar{Q}$  or  $c^* = g^*$  with  $g^* \rightarrow Q\bar{Q}$ . These hard processes are sampled from the well-documented cross-sections [8,9,15], including the direct process and gluon fragmentation process with weights given by the relative magnitudes of the corresponding cross-sections.
- (iii) The *parton cascade* development proceeds then by propagating all partons along classical trajectories until they interact (radiate, coalesce, or hadronize), including the  $Q\bar{Q}$  system as well as the additionally produced partons from initial-state space-like radiation off  $a, b$  and final-state time-like radiation off the  $Q\bar{Q}$  system and the recoiling jet  $d$ . The production of each parton through the hard scattering or radiation is subject to an individual, kinematic-specific formation time  $\Delta t_{p,c} = \gamma/M_p$  where  $1/M_p = 1/\sqrt{k^2}$  is the proper decay time of an off-shell parton with invariant mass  $M_p$  and  $\gamma = E/M_p$  is the Lorentz factor.
- (iv) The *final  $Q\bar{Q}$  quarkonium formation* is traced by evaluating in each infinitesimal step of the collision event the spectrum of coalescence probabilities (29) and (30) from the  $Q$  and  $Q\bar{Q}$  positions and momenta, and testing the values against a random number. At each point in time the total probability determines whether a quarkonium state may be produced, and if so, the relative probabilities of the different states give the weights for which quarkonium state out of the spectrum is formed. If no coalescence occurs, the  $Q$  and  $\bar{Q}$  continue in their evolution as individual particles as in (iii).
- (v) The *emergence of hadrons other than quarkonium* involves the recombination of produced partons into pre-hadronic cluster, using the Ellis-Geiger scheme [32], in which at any point during the cascade development any pair of nearest-neighbor partons is tested whether their mutual separation favors a cluster formation, or whether they proceed in their parton evolution as in (iii). These pre-hadronic clusters decay subsequently into primary hadrons, which in turn if excited or resonant states, can decay into final stable particles according to the particle data tables [33]. Again, each newly produced pre-hadronic cluster as well as emerging hadron becomes a ‘real’ particle only after a characteristic formation time  $\Delta t_{c,h} = \gamma/M_{c,h}$  depending on the invariant mass  $M_{c,h}$  and the energy through  $\gamma = E/M_{c,h}$ . Before that time has passed, a cluster or hadron is considered as a still virtual object that cannot interact incoherently until it has formed according to the uncertainty principle.

---

<sup>‡</sup> The GRV structure function parametrization [31], is used throughout, which describes quite accurately the HERA data even at low  $Q^2$  and very small  $x$ .

(vi) The *beam remnants*, being the unscathed remainders of the initial beam particles (in the present case  $p$  and  $\bar{p}$ ), emerge from reassembling all those remnant primary partons that have been spectators without interactions throughout the evolution. The recollection of those yields two corresponding beam clusters with definite charge, baryon number, energy-momentum and position, as given by the sum of their constituents. These beam clusters decay into final-state hadrons which recede along the beam direction at large rapidities of the beam/target fragmentation regions. Again, individual formation times of the produced hadrons are accounted for.

It is important to realize that the spatial density and the momentum distribution of the particles are intimately connected: The momentum distribution continuously changes through the interactions<sup>§</sup> and determines how the quanta propagate in coordinate space. In turn, the probability for subsequent interactions depends on the resulting local particle density. Consequently, the development of the phase-space densities is a complex interplay, which - at a given point of time - contains implicitly the complete preceding history of the system.

Parameter	Value	Description
$\Delta t$	0.001 fm	time step by which the evolution of the particle system is followed in the hadronic center-of-mass frame.
$\Lambda_{QCD}$	0.29 GeV	QCD scale used in $\alpha_s$ and throughout the perturbative evolution of the parton distributions.
$\mu$	1.0 GeV	mass scale below which the perturbative parton evolution is cut off, if not terminated before by coalescence or hadron formation.
$M_c$	1.35 GeV	value used for charm quark mass
$M_b$	5.0 GeV	value used for bottom quark mass

TABLE II. Parameter values used in the model calculations.

---

<sup>§</sup> For the case of  $pp$  or  $p\bar{p}$  collisions considered in the following, the general variety of particle interactions reduces to only the radiative parton production associated with the evolution before and after the hard scattering, and the parton-hadron conversion through parton-parton recombination or coalescence.

### III. APPLICATION TO $PP(P\bar{P})$ COLLISIONS AT 30 GEV - 14 TEV

For the production of the charmonium and bottomonium  $S$ -wave states  $J/\psi$  and  $\Upsilon$ , respectively, there exists a body of experimental data, both from  $pp$  collisions at the ISR ( $\sqrt{s} = 30\text{--}63$  GeV) and from  $p\bar{p}$  experiments at the Tevatron ( $\sqrt{s} = 1.8$  TeV). Also, the charmonium  $P$ -wave states  $\chi_c$  have been observed, although with larger experimental uncertainty, since these states are only indirectly measured through their radiative decay into  $J/\psi$  (unlike the  $S$ -wave states which due to their narrow resonance character can be observed directly through invariant mass analysis). On the other hand, for radial  $S$ -wave excitations, such as  $\psi'$ ,  $\Upsilon'$ ,  $\Upsilon''$ , data are more scarce, and detailed measurements of  $\chi_b$  as well as of the  $^1S_0$  and  $^1P_1$  states,  $\eta_c$ ,  $\eta_b$ ,  $h_c$ ,  $h_b$ , are not reported at all.

Hence, I will focus primarily on the production of the charmonium states  $J/\psi$  ( $^3S_1$ ) and  $\chi_{cJ}$  ( $^3P_J$ ), as well as the lowest-lying bottomonium state  $\Upsilon$  ( $^3S_1$ ). However, since in the model calculations the production patterns of the various quarkonium states are intimately entwined by the dynamical evolution, I also discuss somewhat the relevance of the other  $S$ -wave and  $P$ -wave states.

#### A. Production cross-sections: postdictions and predictions

The *principal result* of this paper is contained in Fig. 7, which collects the quarkonium production cross-sections for  $J/\psi$ ,  $\chi_c$  and  $\Upsilon$ , and which is posted here forefront as basis for the subsequent analysis of the underlying dynamics in the present approach. Shown in Fig. 7 is the  $p_\perp$ -dependence of the cross-sections around central rapidity at 63 GeV, 1.8 TeV and 14 TeV, as given by eq. (43),

$$\left. \frac{d\sigma}{dp_\perp} \right|_{y=0} = 2p_\perp \left. \frac{d\sigma}{dp_\perp^2} \right|_{y_1+y_2 \leq 1} \quad \text{for } pp(p\bar{p}) \longrightarrow \begin{cases} J/\psi + X \\ \chi_c \rightarrow J/\psi + X \\ \Upsilon + X \end{cases}, \quad (45)$$

multiplied by the leptonic branching ratios  $B(J/\psi \rightarrow \mu^+\mu^-) = 5.97\%$ , and  $B(\Upsilon \rightarrow \mu^+\mu^-) = 2.48\%$ . Confronted are the calculated cross-sections (from eqs. (43) and (44)) with the measured spectra from Refs. [1,34]. In order to allow direct comparison with experimental data, the following quarkonium yields are plotted: The top panel of Fig. 7 displays the production of prompt  $J/\psi$ 's only, with the radiative feed-down from  $\chi_c$ 's as well as from bottom decays subtracted. The middle part reflects the production of  $\chi_c$  summed over all  $J = 0, 1, 2$  states, and implicitly obtained through the amount of  $J/\psi$ 's that result exclusively from the radiative decays of  $\chi_c$  with the branching ratios  $B(\chi_{c0} \rightarrow J/\psi + \gamma) = 6.6 \cdot 10^{-3}\%$ ,  $B(\chi_{c1} \rightarrow J/\psi + \gamma) = 27.3\%$ ,  $B(\chi_{c2} \rightarrow J/\psi + \gamma) = 13.5\%$ . Finally, the bottom panel shows the production of  $\Upsilon$ 's, including the radiative feed-down from the  $\chi_b$  states.

The features of the results in Fig. 7 may be itemized as follows:

- (i) The agreement of the calculated cross-sections for  $J/\psi$ ,  $\chi_c$  and  $\Upsilon$  production with the experimental data at ISR and Tevatron is very good. Not only the  $p_\perp$ -shapes of the cross-sections, but also the overall magnitudes are *postdicted* correctly for ISR and Tevatron. The LHC curves may therefore be seen as quantitative *predictions*. In view of the fact that the dynamics of quarkonium production in the model calculations is essentially parameter-free (aside from the fixed quarkonium radii in Table 1), this success suggests that the combination of PQCD parton evolution with bound-state formation via coalescence may in fact be a reasonable visualization of the underlying physics.
- (ii) The overall pattern of charmonium and bottomonium production is quite similar, although with important differences in detail. The comparison of the  $J/\psi$  and  $\Upsilon$  production reveals a ‘flattening’ of the  $p_\perp$ -spectra due to the larger quark mass in the latter case (c.f. Table 2), and, connected with this, a much smaller size of the  $\Upsilon$  as compared to the  $J/\psi$  (c.f. Table 1). The confrontation of the  $\chi_c$  and  $J/\psi$  spectra implies a softer, i.e. ‘steeper’,  $p_\perp$  tail in the  $\chi_c$  production, which again is plausible due to the larger size of the  $\chi_c$  states. The ‘flattening’ indicates a power-behavior in the transverse energy  $\sqrt{4M_Q^2 + p_\perp^2}$  rather than in the transverse momentum  $p_\perp$  itself.
- (iii) Most prominent in the charmonium sector is  $\chi_c$  production, leading also to a strong  $\chi_c$  component in the inclusive  $J/\psi$  yield through radiative feed-down  $\chi_c \rightarrow J/\psi + \gamma$ . In fact, the calculations show that more than 30 % of the total  $J/\psi$  yield originates from  $\chi_c$  decays. On the bottomonium sector this pattern is repeated, as the model calculations indicate. Again, the  $\chi_b$ 's provide the largest yield, however, they do not contribute as strongly to the  $\Upsilon$  population as in the corresponding case of  $\chi_c$  and  $J/\psi$ . This is due to the larger quark mass which leads to a kinematic suppression at large  $p_\perp$ .

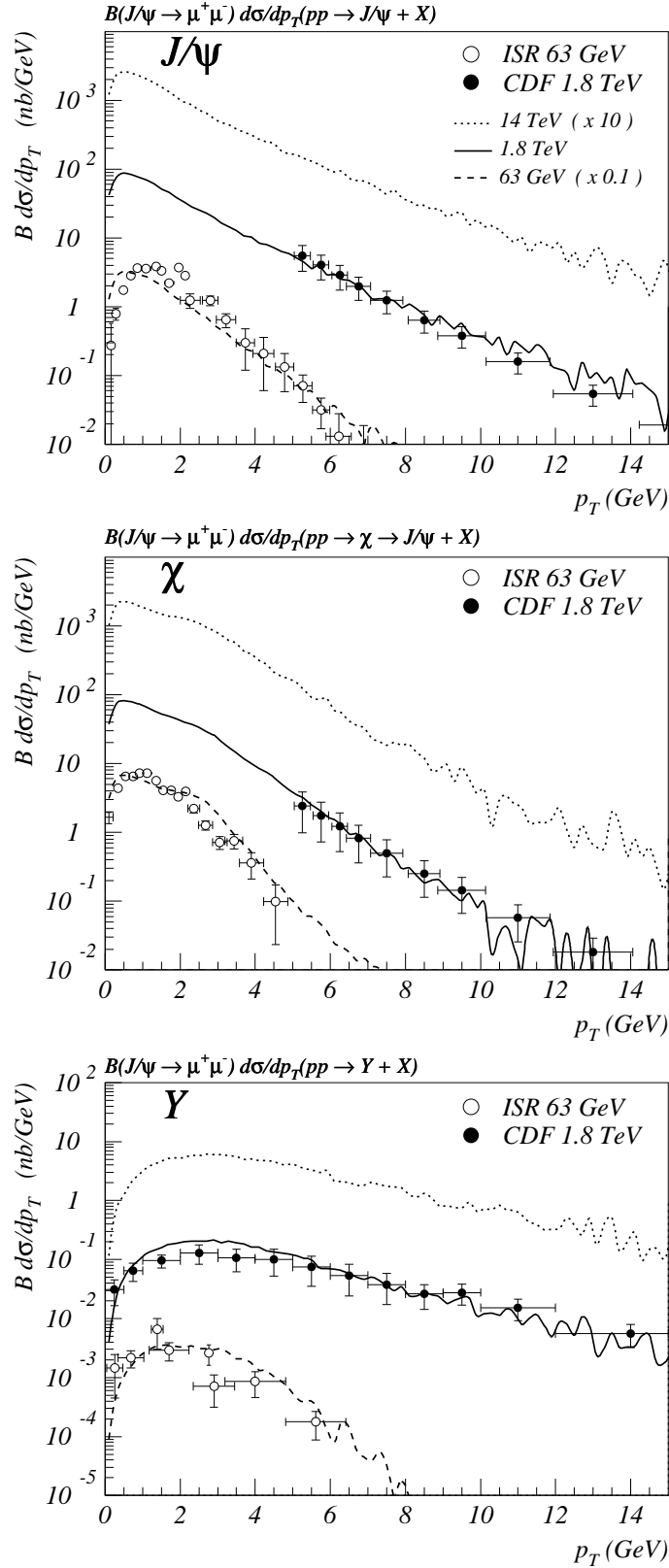


FIG. 7. Comparison of calculated and measured cross-sections for quarkonium production around central rapidity at 63 GeV, 1.8 TeV and 14 TeV. Top part includes prompt  $J/\psi$ 's only, with the radiative feed-down from  $\chi_c$ 's as well as from bottom decays subtracted. Middle part shows  $\chi_c$  production summed over all  $J = 0, 1, 2$  states, identified from  $J/\psi$ 's that result exclusively from the  $\chi_c$  decays. Bottom part contains  $\Upsilon$ 's, including the radiative feed-down from the  $\chi_b$  states. For better distinction, the cross-sections have been scaled by factors of 0.1 (63 GeV), 1 (1.8 TeV) and 10 (14 TeV). The full curves are the model results. The data points are from Ref. [34] for ISR at 63 GeV and from Ref. [1] for Tevatron at 1.8 TeV.

In view of the non-trivial physics of quarkonium production as discussed in Sec. I, the good agreement of the model calculations with the available data immediately poses the the question,

*Why does this space-time description, which combines PQCD parton production and evolution with a simple coalescence model, agree so well with experiment?*

More specifically, there are three main issues to be examined in the following, namely,

- *Initial  $Q\bar{Q}$  production:* What is the underlying production pattern, in particular, the relative importance of color-singlet and color-octet contributions?
- *Parton evolution:* How does the PQCD evolution and the associated gluon radiation affect the quarkonium yield?
- *Coalescence:* How does the space-time development of the initial  $Q\bar{Q}$  proceed and what are the characteristics of the final  $Q\bar{Q}$  upon coalescence?

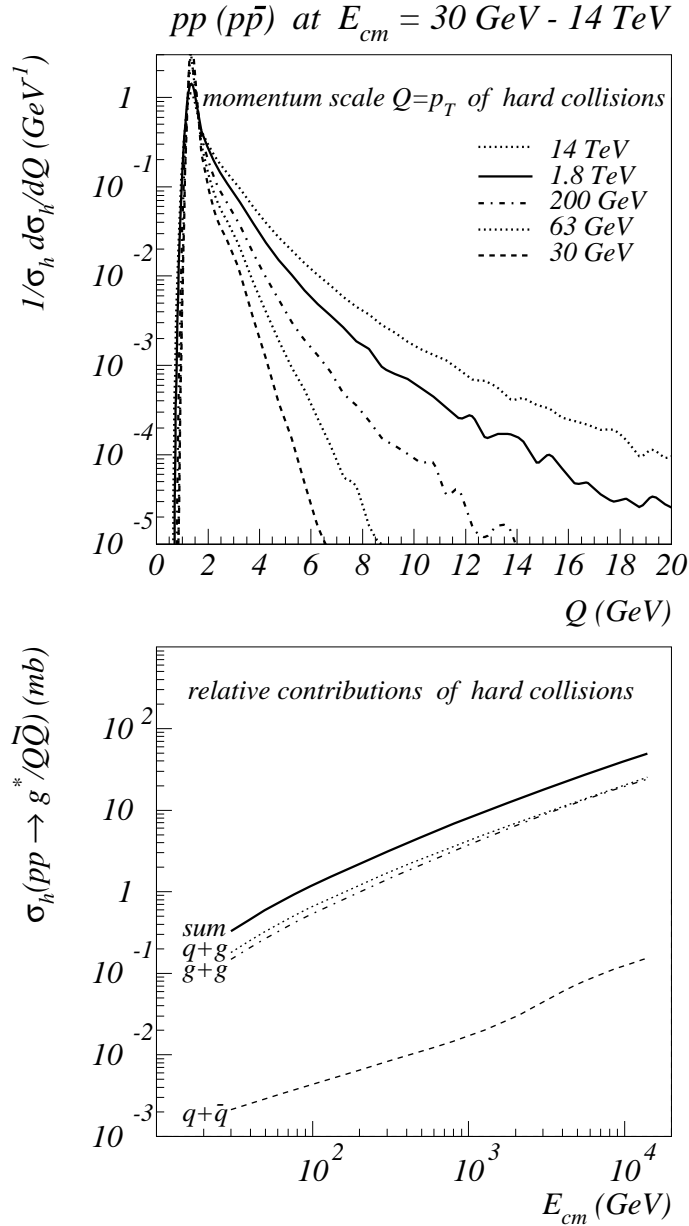


FIG. 8. *Top panel:* Distribution of  $Q^2$  values for the  $pp$  ( $p\bar{p}$ ) energy range  $\sqrt{s} = 30 \text{ GeV} - 14 \text{ TeV}$ , where  $Q \equiv p_{\perp}$  represents the momentum transfer at the hard vertex  $ab \rightarrow c^*d$  of Fig 2. *Bottom panel:* Integrated partonic cross-section for the production of the initial  $Q\bar{Q}$  from the hard vertex  $ab \rightarrow c^*d$  (directly, or via gluon fragmentation) in the energy range  $\sqrt{s} = 30 \text{ GeV} - 14 \text{ TeV}$ .

In the following Subsections these questions are addressed and discussed in detail. Beforehand, I would like to draw attention to Fig. 8, which may serve to further some intuition for the beam-energy ( $\sqrt{s}$ ) dependence of quarkonium production and the relative importance of contributing partonic production processes. The top part of Fig. 8 displays the distribution of  $Q^2 \equiv p_\perp^2$  values for the  $pp$  ( $p\bar{p}$ ) beam energies 30 GeV - 14 TeV. It reflects the typical momentum transfers at the hard vertex  $ab \rightarrow c^*d$ , where  $a, b, d = g, q, \bar{q}$  and  $c^* = Q\bar{Q}$  (Fig. 2a) or  $c^* = g$  with  $g \rightarrow Q\bar{Q}$  (Fig. 2b). As expected, there is a substantial increase in the mean  $Q^2$ , accompanied by an increasingly prominent power-law tail, as one moves from ISR energy 30 GeV up to LHC energy 14 TeV. The immediate consequences are, firstly, an enlarging of the kinematic region for producing heavier quarkonium states, and secondly, the increasing importance of gluon radiation, the role of which I shall discuss in detail later. The bottom part of Fig. 8 shows the beam-energy dependence of the integrated partonic cross-section for the production of the initial  $Q\bar{Q}$  from the hard vertex  $ab \rightarrow c^*d$  (directly, or via gluon fragmentation). Three features are self-evident here. First, the cross-section rises by almost two orders of magnitude in the range 30 GeV - 14 TeV. Second, the channel  $ab = q\bar{q}$  of light  $q\bar{q}$  annihilation is down by 2 orders of magnitude, and is therefore completely irrelevant in the energy range considered here. Third, the contributions of  $ab = qg$  and  $ab = gg$  are about equal in magnitude throughout, with the  $qg$ -channel slightly dominating. This is a very important property that is often overlooked, because one would naively expect that the  $gg$ -channel dominates by far due to the strong presence of low- $x$  gluons in the protons. However, collisions of low- $x$  gluons are suppressed in the  $Q\bar{Q}$  production, because of the failure to overcome the mass threshold.

## B. Properties of color-singlet versus color-octet contributions

In addressing the first of the above issues, namely the relative importance of color-singlet versus color-octet contributions to the final-state quarkonium yield, recall from the Sec. I, that historically the ‘color-singlet model’ [7–9] did very well at ISR energies and below, but underpredicts badly the quarkonium productions at the Tevatron by more than an order of magnitude, and thereby suggesting a strong ‘color-octet mechanism’ [4,15,16] contributing at very high energies.

In the present approach, both color-singlet and color-octet production of the initial  $Q\bar{Q}$  are self-consistently included, by determining the relative probabilities for singlet and octet production from the respective weights of the hard  $Q\bar{Q}$ -production cross-sections. It is important to stress again that an initial singlet (octet)  $Q\bar{Q}$  pair produced by the hard parton collision does not necessarily result in a final  $Q\bar{Q}$  with the same quantum numbers upon coalescence, because the emission of gluons during the evolution changes the color state (and in principle also spin and angular momentum) of the pair. In fact, since in the present approach, the final  $Q\bar{Q}$  has to be in a color-singlet state in order to coalesce to a quarkonium bound-state, this is a crucial necessity to be able to incorporate both singlet and octet production of initial  $Q\bar{Q}$  pairs. Figs. 9 - 11 separate the color-singlet and color-octet contributions and discriminate their characteristic features.

Fig. 9 compares the relative proportions of the various included charmonium states at Tevatron energy  $\sqrt{s} = 1.8$  TeV (the pattern is very similar on the bottomium sector, not shown here). The top panel contains the realistic case with proper admixtures of both color-singlet and -octet contributions, and shows a strong  $J/\psi$  component, yet being dominated by  $\chi_c$  productions with a ratio  $P(J/\psi)/P(\chi_c) \approx 2$ . The middle (bottom) panel exhibits the contributions from initial  $Q\bar{Q}$  color-singlet (color-octet) pairs alone. The patterns are strikingly different, as is already visible in the earlier Fig. 4. Color-singlet production of the initial  $Q\bar{Q}$  results to largest extent in  $\chi_c$ -formation (mostly  $\chi_{c1}$ ), whereas  $J/\psi$ ,  $\eta_c$  and  $h_c$  are down by far more than an order of magnitude. Contrary to that, when the initial  $Q\bar{Q}$  is produced in a color-octet, the situation is almost reversed.  $J/\psi$  production is the largest among the individual states, and is about equal to the sum of all three  $\chi_c$  states.

Figs. 10 and 11 detail the beam energy ( $\sqrt{s}$ ) dependence of color-singlet and -octet contributions for the charmonium and bottomium sector, respectively. In Fig. 10 the relative probabilities for  $\chi_c$  and  $J/\psi$  production are shown in the top panel, whereas the actual cross-sections are plotted in the bottom panel – both against the  $pp$  ( $p\bar{p}$ ) center-of-mass energy  $E_{cm} = \sqrt{s}$ . Correspondingly, Fig. 11 depicts the behavior of  $\chi_b$  versus  $\Upsilon$  production. The fat lines are the sum of color-singlet and color-octet contributions, the thin dashed (dotted) lines represent the color-singlet (-octet) contributions alone. From Fig. 10 one reads off that, in the present model, the color-singlet component of  $J/\psi$  is almost constant with  $E_{cm}$ , whereas the color-octet contribution rises strongly with increasing  $E_{cm}$ . At the same time color-singlet and -octet contributions to  $\chi_c$  are of the same order of magnitude, and decrease with  $E_{cm}$ . As a result, at ISR energies 30 - 63 GeV, the  $J/\psi$  production is highly suppressed as compared to the  $\chi_c$  yield, at Tevatron energy 1.8 TeV, the two channels become almost comparable, and at LHC energy 14 TeV, they become about equal. A similar pattern is seen in Fig. 11 for  $\chi_b$  and  $\Upsilon$ , however with an even more pronounced energy dependence. Again,  $\chi_b$  production is by far favored over  $\Upsilon$  formation at lower energies, but now already at Tevatron energy the two states are equally populated, and at LHC energy the  $\Upsilon$  production even dominates by a factor of  $\simeq 1.5$ .



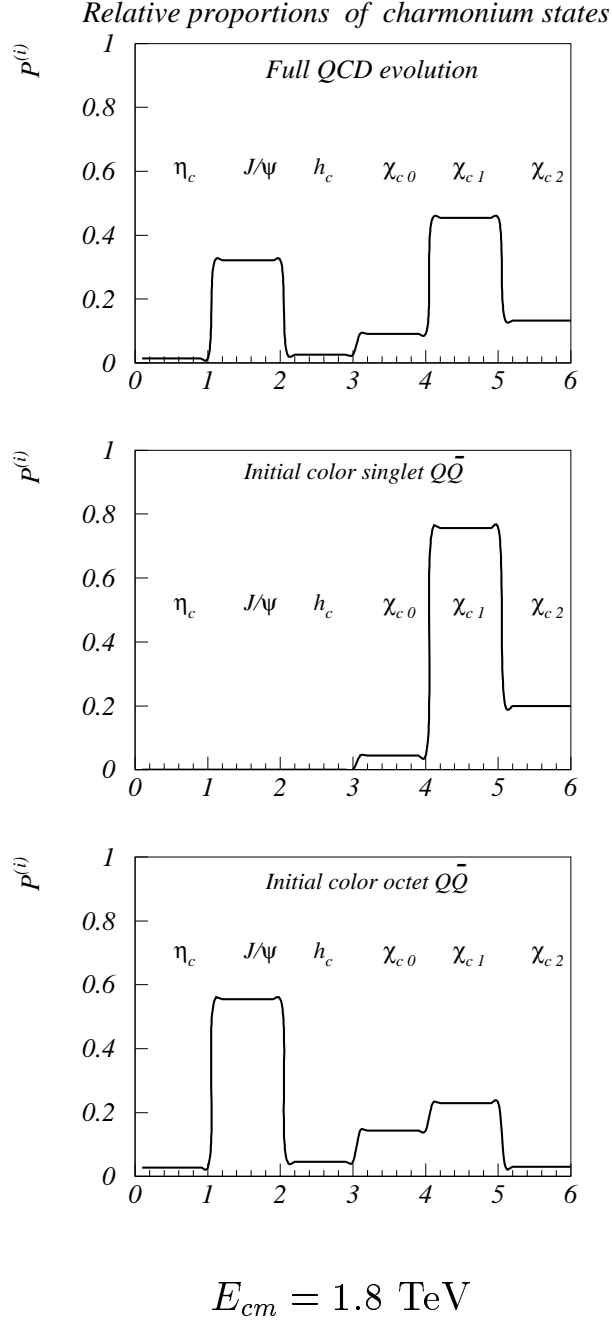


FIG. 9. Relative proportions of the various included charmonium states at Tevatron energy  $\sqrt{s} = 1.8 \text{ TeV}$ : *top panel* contains the realistic case with proper admixtures of both color-singlet and color-octet contributions, *middle panel* exhibits the contributions from initial  $Q\bar{Q}$  color-singlet pairs alone, whereas *bottom panel* displays the contributions from initial  $Q\bar{Q}$  color-octet pairs only.

### Singlet vs. octet contribution to $J/\psi$ and $\chi_c$

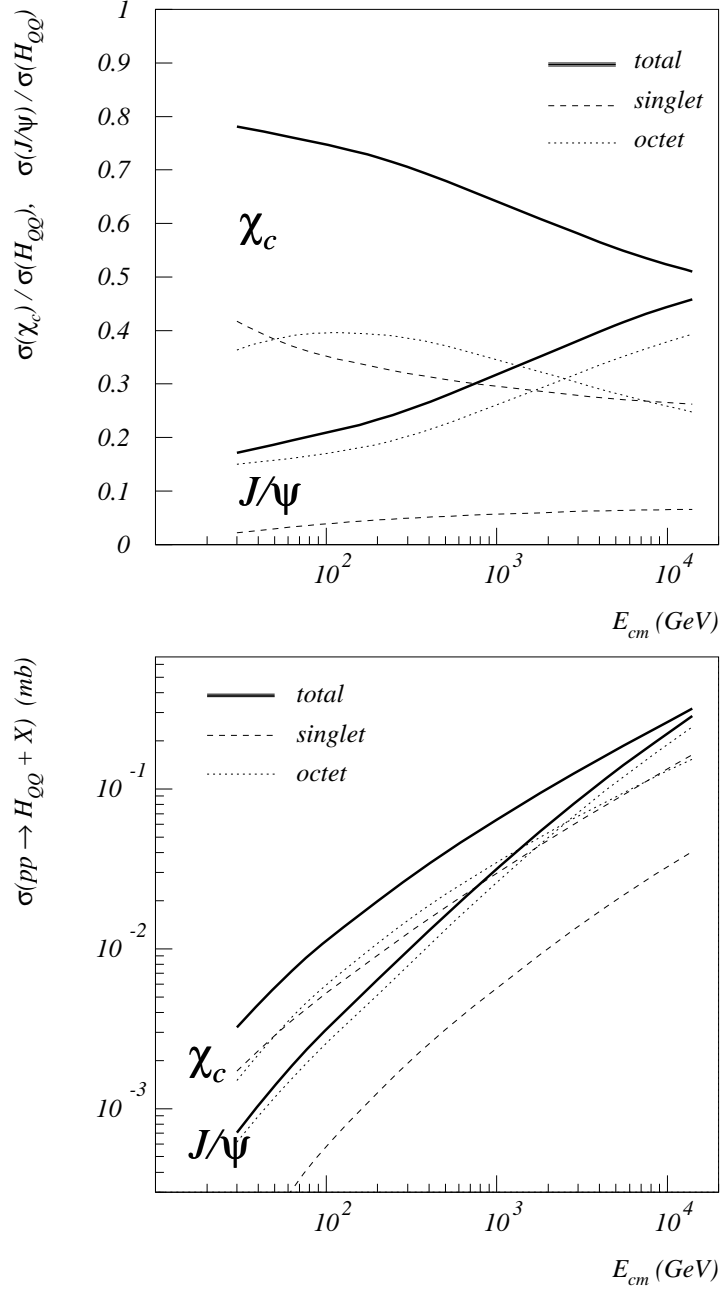


FIG. 10. Relative probabilities for  $\chi_c$  and  $J/\psi$  production (top), and corresponding cross-sections (bottom) versus  $pp$  ( $p\bar{p}$ ) center-of-mass energy  $E_{cm} = \sqrt{s}$ . The fat lines are the sum of color-singlet and color-octet contributions, the thin dashed (dotted) lines represent the color-singlet (color-octet) contributions alone.

### Singlet vs. octet contribution to $Y$ and $\chi_b$

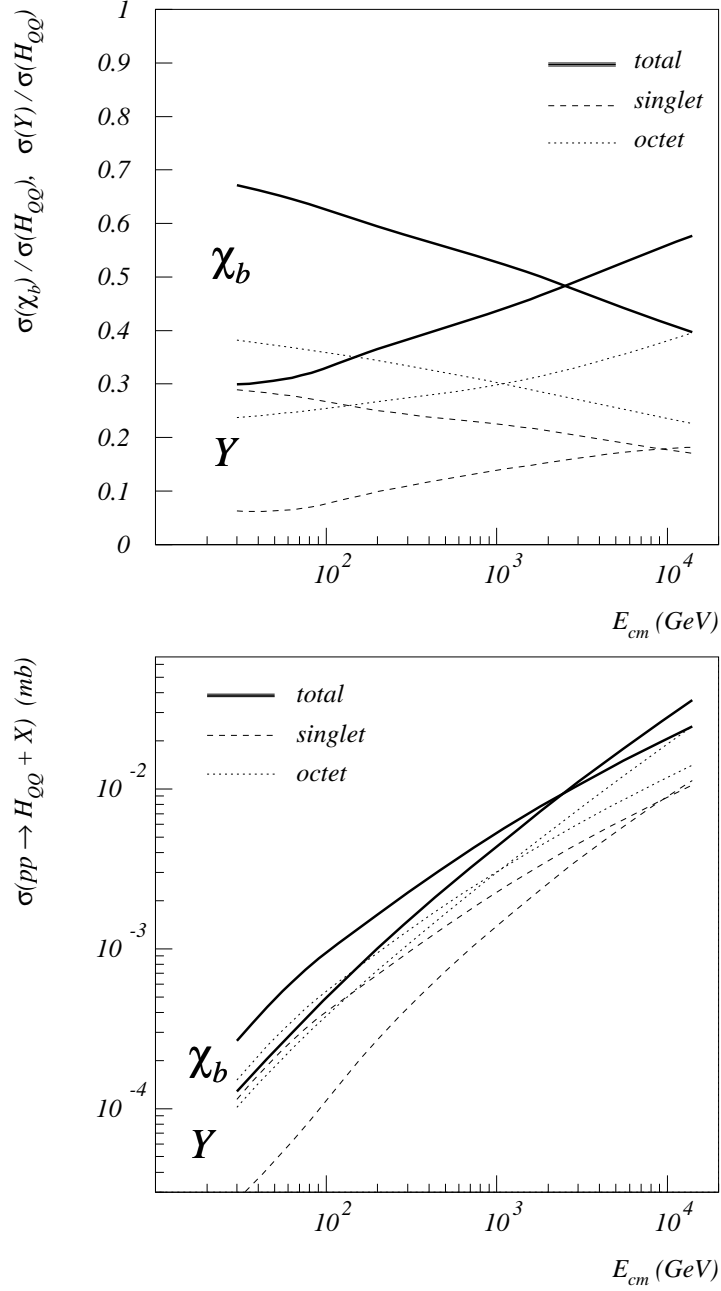


FIG. 11. Relative probabilities for  $\chi_b$  and  $Y$  production (top), and corresponding cross-sections (bottom) versus  $pp$  ( $p\bar{p}$ ) center-of-mass energy  $E_{cm} = \sqrt{s}$ . The fat lines are the sum of color-singlet and color-octet contributions, the thin dashed (dotted) lines represent the color-singlet (color-octet) contributions alone.

### C. Importance of parton evolution and gluon radiation

Next, I turn to the second question raised above which concerns the importance and effects of gluon radiation during the PQCD evolution. As illustrated in Fig.2, gluon bremsstrahlung from both the virtual gluon (in case of the gluon fragmentation process) and from the produced  $Q\bar{Q}$  pair are included within the standard DGLAP evolution plus angular-ordering in the leading log approximation [20]. This (multi-)gluon emission is a most important aspect in the present approach. Firstly, it changes the color-state of the  $Q\bar{Q}$  which makes it possible for an initial  $Q\bar{Q}$  color-octet to evolve into a final  $Q\bar{Q}$  color-singlet and to coalesce to a physical bound-state. \*\* Without gluon emission, only those  $Q\bar{Q}$  pairs that are initially produced as color-singlets could contribute to quarkonium formation. Secondly, gluon radiation causes significant energy loss of the  $Q\bar{Q}$  system at high energy, causing the relative momentum of the pair to be smaller in the mean, and their relative distance to increase slower. In effect, this dynamical feature enhances the probability for coalescence, since configurations with very small relative momentum and separation are strongly favored (c.f. Fig. 6). In other words, the presence of gluon radiation is crucial, because it allows the natural inclusion of both color-singlet and color-octet initial  $Q\bar{Q}$  pairs to evolve into quarkonium, and because the coalescence of final  $Q\bar{Q}$  systems is more likely to occur after sufficient gluon radiation to reduce the relative velocity to a value commensurate with the non-relativistic kinematics of the accessible quarkonium bound-states.

Fig. 12 clearly displays the effect of gluon radiation in the model calculations. Confronted are the production cross-sections (45) for the realistic scenario including gluon emission during the PQCD evolution which are the same as in Fig. 7 (fat lines), with the corresponding cross-sections obtained by switching off all gluon radiation (thin lines). The comparison of the calculations with and without multiple gluon emission reveals two substantial differences. First, the overall magnitude in the case without gluon radiation is significantly lower by a factor of about 3 for  $J/\psi$  and  $\Upsilon$ , but only slightly less for  $\chi_c$ . Second, the shapes of the  $S$ -wave states  $J/\psi$  and  $\Upsilon$  are quite different in the two scenarios, indicating a softer, i.e. steeper,  $p_\perp$ -dependence in the no-radiation case. The shape of the cross-section for the  $P$ -wave  $\chi_c$ , on the other hand, shows a suppression at low  $p_\perp$  in the case without gluon radiation, but is hardly affected at large  $p_\perp$ .

Both these points can be intuitively understood. The substantial under-population of  $J/\psi$  and  $\Upsilon$  in the no-radiation case is due to the fact that without gluon emission, only the color-singlet component of initial  $Q\bar{Q}$  production contributes, because color-octet pairs have no chance to convert into a final-state color-singlet, as is necessary to form quarkonium. Since at  $\sqrt{s} = 1.8$  TeV the color-singlet cross-sections are smaller than the color-octet counterparts (c.f. Figs. 10 and 11), the yield of  $J/\psi$  and  $\Upsilon$  is naturally underestimated. On the other hand, the  $\chi_c$  production is much less deviating in the two cases, because here color-singlet and color-octet cross-sections are roughly of equal magnitude.

The main lesson learned from Fig. 12 is that the neglect of gluon radiation results in quarkonium cross-sections which are incompatible with the data shown earlier in Fig. 7, both with respect to the absolute yield and the shape of the  $p_\perp$ -dependence.

Fig. 13 further confirms the importance of multi-gluon emission. Plotted are the probability distributions of the number of gluons being emitted during the PQCD evolution between the hard vertex  $ab \rightarrow c^*d$  of Fig. 2, up to the point of coalescence to a quarkonium bound-state. The full (dashed) histograms are for charmonium (bottomonium) at  $pp$  ( $p\bar{p}$ ) center-of-mass energies 63 GeV (top), 1.8 TeV (middle), and 14 TeV (bottom). One observes that  $b\bar{b}$  evolution is generally accompanied by a larger amount of gluon radiation than  $c\bar{c}$ , an effect that increases with energy. Even at ISR energy 63 GeV, gluon radiation is non-negligible, with mean values of  $\langle N_g \rangle = 1.4$  (1.7) for  $c\bar{c}$  ( $b\bar{b}$ ). At Tevatron energy 1.8 TeV, the mean number of gluons emitted per  $Q\bar{Q}$  system are  $\langle N_g \rangle = 1.9$  (4.7) for  $c\bar{c}$  ( $b\bar{b}$ ), and at LHC energy 14 TeV, one has  $\langle N_g \rangle = 2.1$  (5.8). This shows that even at ISR energy 63 GeV, gluon radiation is non-negligible, and that it is most essential at Tevatron and LHC.

---

\*\* Notice that a color-octet  $Q\bar{Q}$  produced in a  $^3S_1$  state must radiate at least two gluons in order to convert into a color-singlet state with quantum numbers of  $J/\psi$  or  $\Upsilon$ . On the other hand, if it is produced in a  $3^3P_J$  state, the emission of only one gluon is necessary to form a  $\chi_{cJ}$  or  $\chi_{bJ}$ .

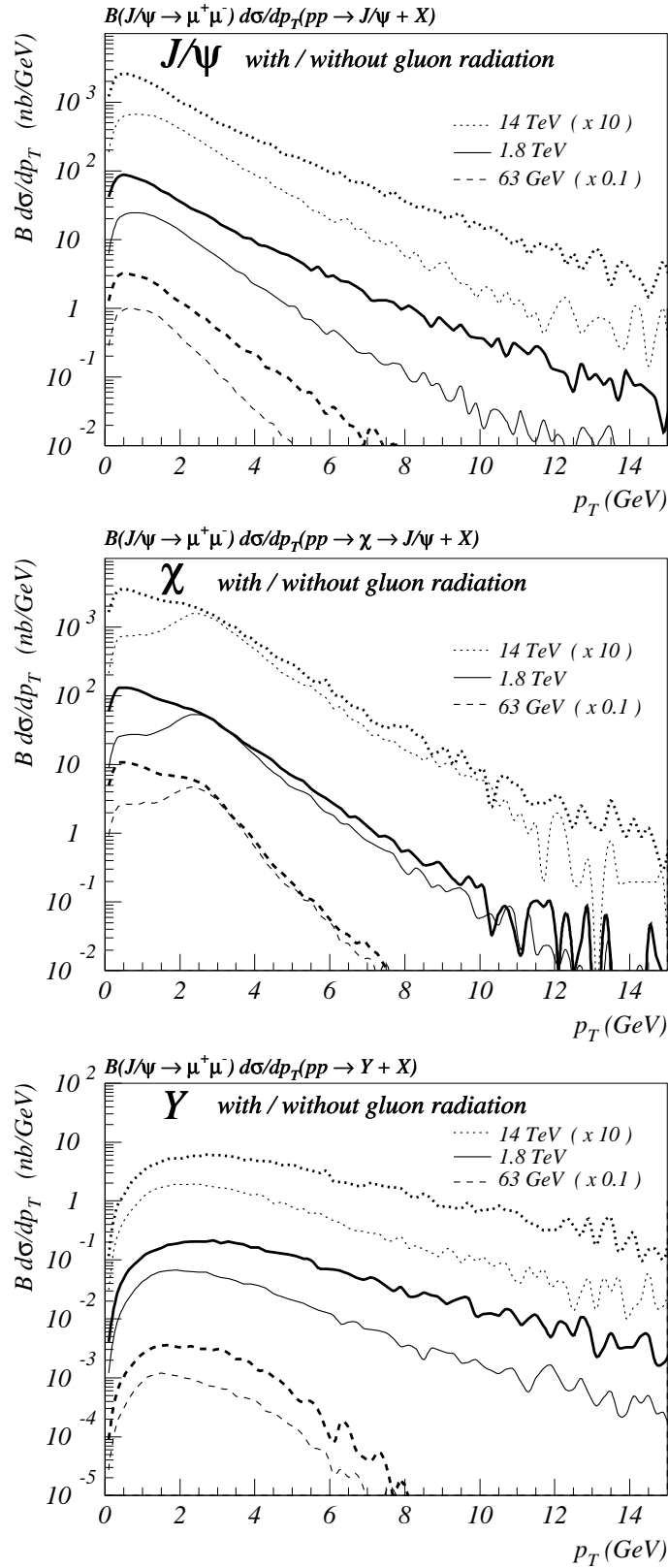


FIG. 12. Quarkonium production cross-sections of the previous Fig. 7 revisited: Fat lines represent the realistic scenario including gluon emission during the PQCD evolution, whereas thin lines correspond to the no-radiation scenario with all gluon radiation switched off. Top part includes prompt  $J/\psi$ 's only, middle part shows  $\chi_c$ 's from radiative  $\chi_c \rightarrow \gamma + J/\psi$ , and bottom part contains  $\Upsilon$ 's, including the radiative feed-down from the  $\chi_b$  states.

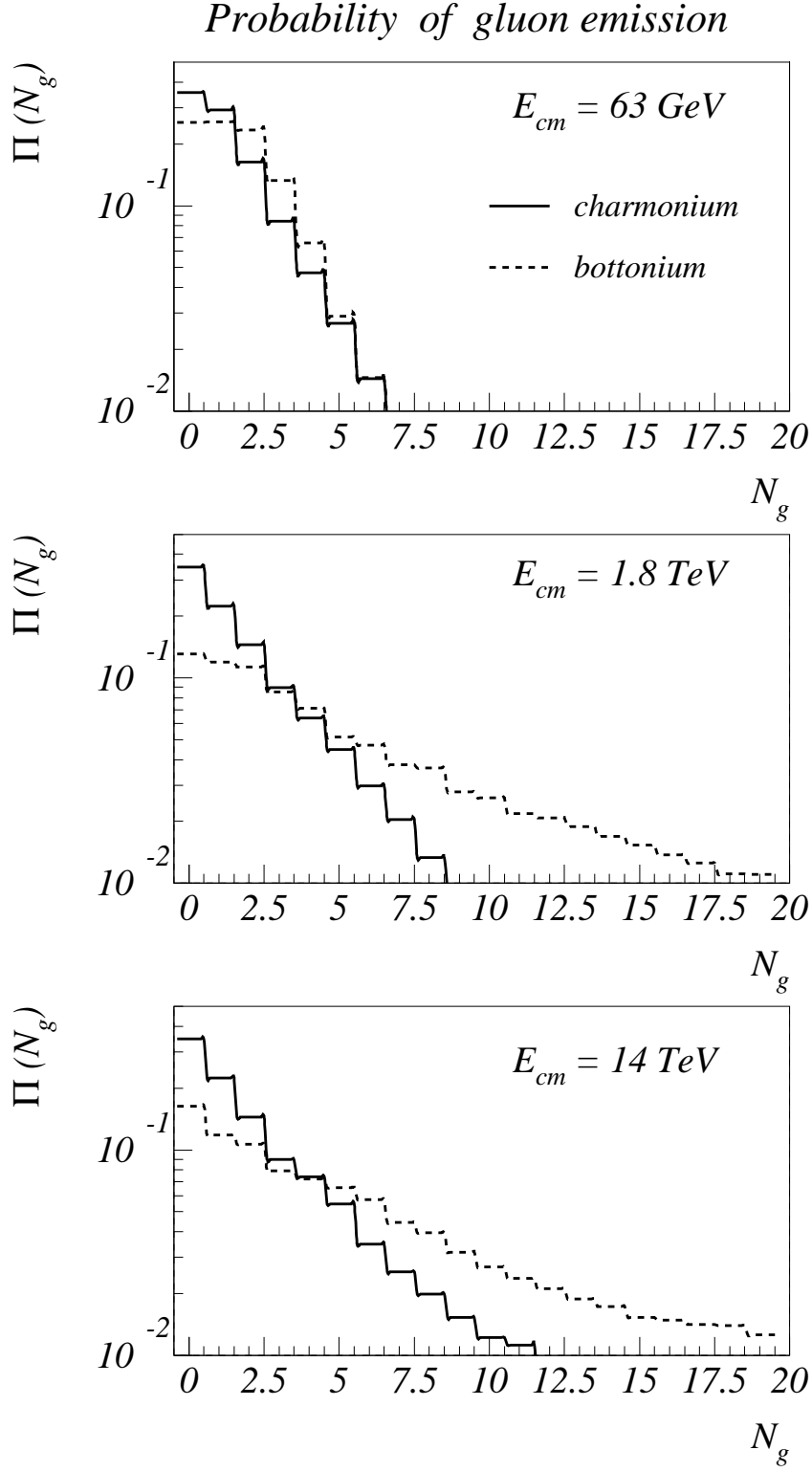


FIG. 13. Probability distributions of the average number of gluons being emitted during the PQCD evolution between the hard vertex  $ab \rightarrow c^*d$  of Fig. 2, up to the point of coalescence to a quarkonium bound-state. The full (dashed) histograms are for charmonium (bottomonium) at  $pp$  ( $p\bar{p}$ ) center-of-mass energies 63 GeV (top), 1.8 TeV (middle), and 14 TeV (bottom).

### D. Characteristics of the space-time development

I finally address the third and last question raised at the end of Sec. III.A, namely, how does the time evolution of the  $Q\bar{Q}$  system proceed after being initially produced either directly at the hard vertex (Fig. a), or by virtual gluon decay (Fig. 2b), as it propagates in space up to the point where it either forms a bound-state, or ends up in other hadrons as open charm, respectively bottom. In view of the preceding discussions, I wish to detail some characteristic space-time features that are related to the issues of multi-gluon emission and color-singlet/color-octet processes.

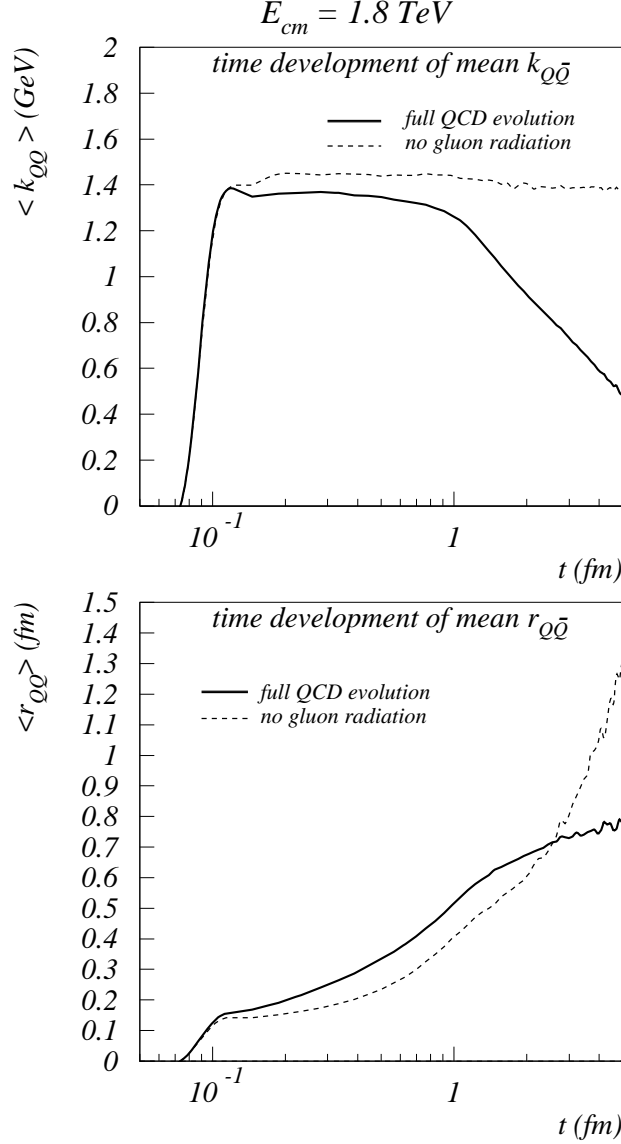


FIG. 14. Time-evolution of the average relative  $Q\bar{Q}$ -momentum  $k_{Q\bar{Q}} \equiv \langle |\mathbf{k}_Q - \mathbf{k}_{\bar{Q}}| \rangle$  (top) and of the average  $Q\bar{Q}$ -separation  $r_{Q\bar{Q}} \equiv \langle |\mathbf{r}_Q - \mathbf{r}_{\bar{Q}}| \rangle$  (bottom). Solid curves represent the ‘full QCD evolution’ including gluon radiation, and dashed curves correspond to ‘free propagation’ without gluon radiation. The plots refer to charmonium production at 1.8 TeV and include only those  $Q\bar{Q}$  that actually end up as final charmonium states.

Fig. 14 vividly illustrates the different time-evolution patterns for the ‘full QCD evolution’ including gluon radiation (solid curves) and the ‘free propagation’ without gluon radiation (dashed curves), here exemplarily depicted for charmonium production at Tevatron energy 1.8 TeV. Only those  $Q\bar{Q}$  are included in the plots that actually end up as final charmonium states, i.e., open charm production has been subtracted. The top panel shows the change of the average relative momentum  $k_{Q\bar{Q}} \equiv \langle |\mathbf{k}_Q - \mathbf{k}_{\bar{Q}}| \rangle$  of  $Q$  and  $\bar{Q}$ , as a function of time in the hadronic center-of-mass frame. The bottom panel displays the corresponding time-dependence of the relative separation of  $Q$  and  $\bar{Q}$  in the pair rest-frame,  $r_{Q\bar{Q}} \equiv \langle |\mathbf{r}_Q - \mathbf{r}_{\bar{Q}}| \rangle$ . The two plots confirm what was mentioned already earlier, namely that multiple gluon emission leads to a significant energy loss which results in a drop<sup>††</sup> of the relative momentum  $k_{Q\bar{Q}}$  (transverse momentum broadening is comparably ineffective). The natural consequence is a slower time change in the relative pair distance  $r_{Q\bar{Q}}$  in the case with gluon radiation. Without the emission of gluons, the  $Q$  and  $\bar{Q}$  do not alter their initially obtained momentum and propagate classically in free space, which leads to a faster growth in their spatial relative separation.

This behavior has interesting consequences for the coalescence process and the resulting quarkonium yield. As is evident from the previous Fig. 6,  $Q\bar{Q}$  configurations with small  $r_{Q\bar{Q}}$  and small  $k_{Q\bar{Q}}$  have the largest coalescence probabilities, and hence are strongly preferred in the formation of quarkonium bound-states. This in turn explains why in Fig. 12 the no-radiation scenario gives a lower quarkonium cross-section than the case with gluon radiation.

Fig. 15 exhibits, again for the charmonium sector at 1.8 TeV, further striking differences between the ‘full QCD evolution’ including gluon radiation, and the ‘free propagation’ without gluon emission. The top part shows the time rate of change of the probability for  $Q\bar{Q}$  bound-state formation, versus the probability for  $Q$  and  $\bar{Q}$  to disappear individually in open charm (i.e., in other charmed hadrons by recombination with partons from the rest of the  $p\bar{p}$  event). The bottom part depicts for those  $Q\bar{Q}$  pairs that indeed form bound-states, the time-dependence of the individual coalescence probabilities  $\langle \Pi^{(i)}(t) \rangle$  for the spectrum of charmonium states  $i = {}^1S_0, {}^3S_1, {}^1P_1, {}^3P_J$ . Both plots exhibit very different shapes for the two cases, with and without gluon radiation. Although this time-development is not directly accessible in experiments, one may think of sensible observables that reflect some of these features and would allow to study the space-time structure by indirect measurement.

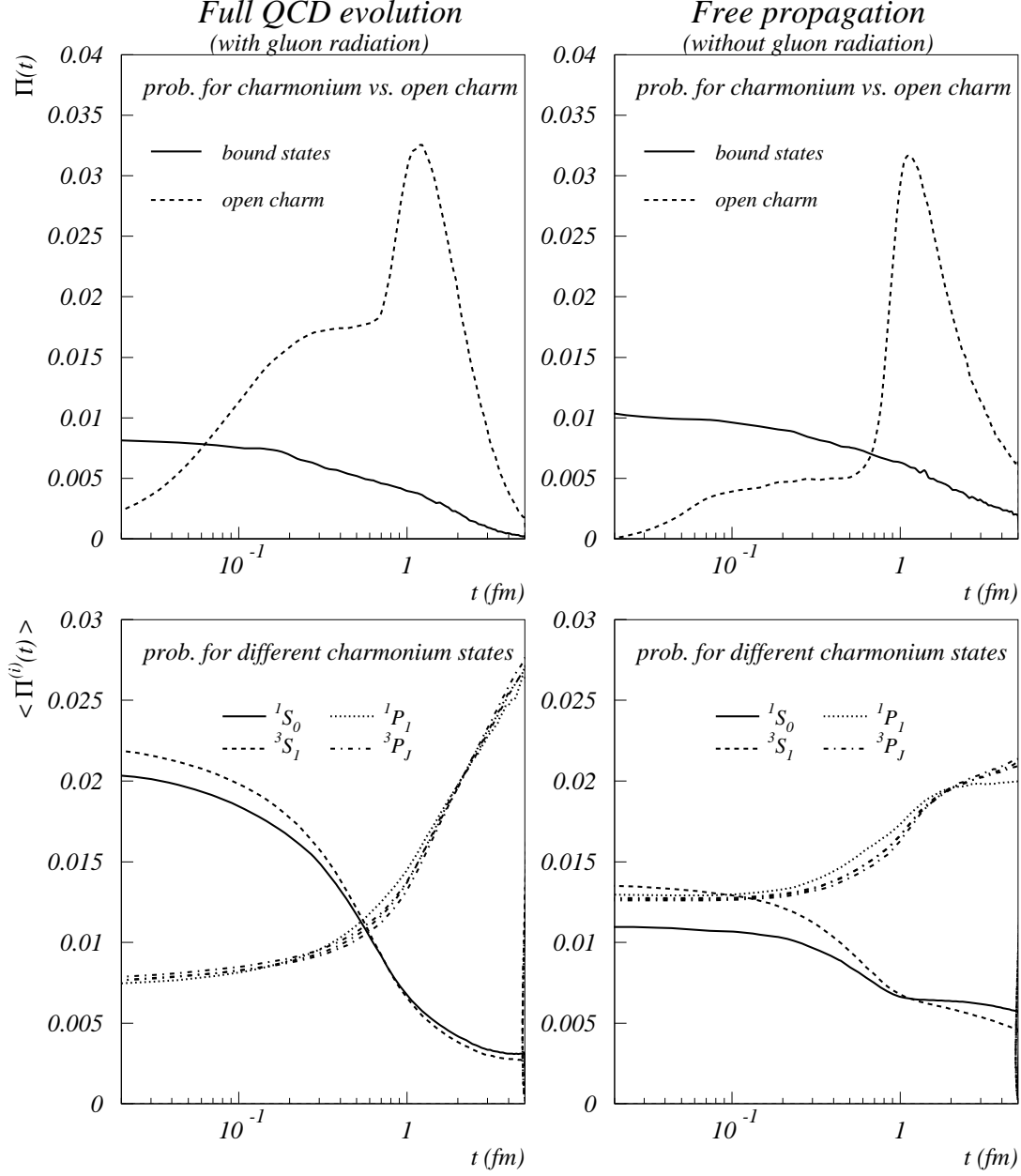
Finally, Fig. 16 gives an instructive summary of the space-time history that the initially produced  $Q\bar{Q}$  pairs have experienced on their way to coalescence as final  $Q\bar{Q}$  color-singlet systems. Again, I choose as example the charmonium sector at  $p\bar{p}$  center-of-mass energy of 1.8 TeV. The left side shows the distributions in relative separation  $r_{ini}$ , relative momentum  $k_{ini}$  and invariant mass  $M_{ini}$  of the  $Q\bar{Q}$  pair upon production, and the right side displays the corresponding spectra with respect to  $r_{fin}$ ,  $k_{fin}$  and  $M_{fin}$  of the final  $Q\bar{Q}$  upon coalescence to charmonium bound-states.

The plots are rather self-evident and in line with intuitive expectations: The initial  $Q$  and  $\bar{Q}$  are highly localized with a mean spatial extent of  $\sim 10^{-2} fm$ , whereas the final  $Q\bar{Q}$  pair has a much larger typical size, being of the order of the size of the charmonium states (c.f. Table 1). On the other hand, the initial and final spectra in the relative  $Q\bar{Q}$  momentum show a reverse pattern, namely a significantly narrower distribution of the final  $Q\bar{Q}$  momentum upon coalescence, being the cumulate effect of gluon radiation that decreases that decreases the originally obtained relative momentum of the  $Q\bar{Q}$  when it was produced initially. Similarly, the mass spectrum of the initial  $Q\bar{Q}$ , being related to the distribution of  $Q^2$  values upon production, spreads out to masses well above 10 GeV, although exponentially damped. The mass distribution of the final  $Q\bar{Q}$ , on the other hand, is concentrated in its mean around the 3 - 4 GeV region, where the charmonium states lie.

---

<sup>††</sup> It should be noted that the pronounced curvature of  $k_{Q\bar{Q}}$  around 1 fm arises as a consequence of the formation time of emitted gluons,  $t_{form} \propto E_g/k_{\perp g}^2$ . Since the bulk of bremsstrahlung is associated with low-energy gluons, the cumulate effect of these latter on  $k_{Q\bar{Q}}$  becomes significant only after the typical formation time  $\gtrsim 1 fm$ .





$$E_{cm} = 1.8 \text{ TeV}$$

FIG. 15. Characteristics of the space-time evolution of the ‘full QCD evolution’ including gluon radiation, and the ‘free propagation’ without gluon emission for charm production at  $p\bar{p}$  center-of-mass energy of 1.8 TeV. *Top part*: time-development of the probability for  $Q\bar{Q}$  bound-state formation, versus the probability for  $Q$  and  $\bar{Q}$  to hadronize in open charm. *Bottom part*: time-dependence of the individual coalescence probabilities  $\langle \Pi^{(i)}(t) \rangle$  for the spectrum of charmonium states  $i = ^1S_0, ^3S_1, ^1P_1, ^3P_J$ . Included are only those  $Q\bar{Q}$  pairs that indeed form bound-states, open charm production is subtracted.

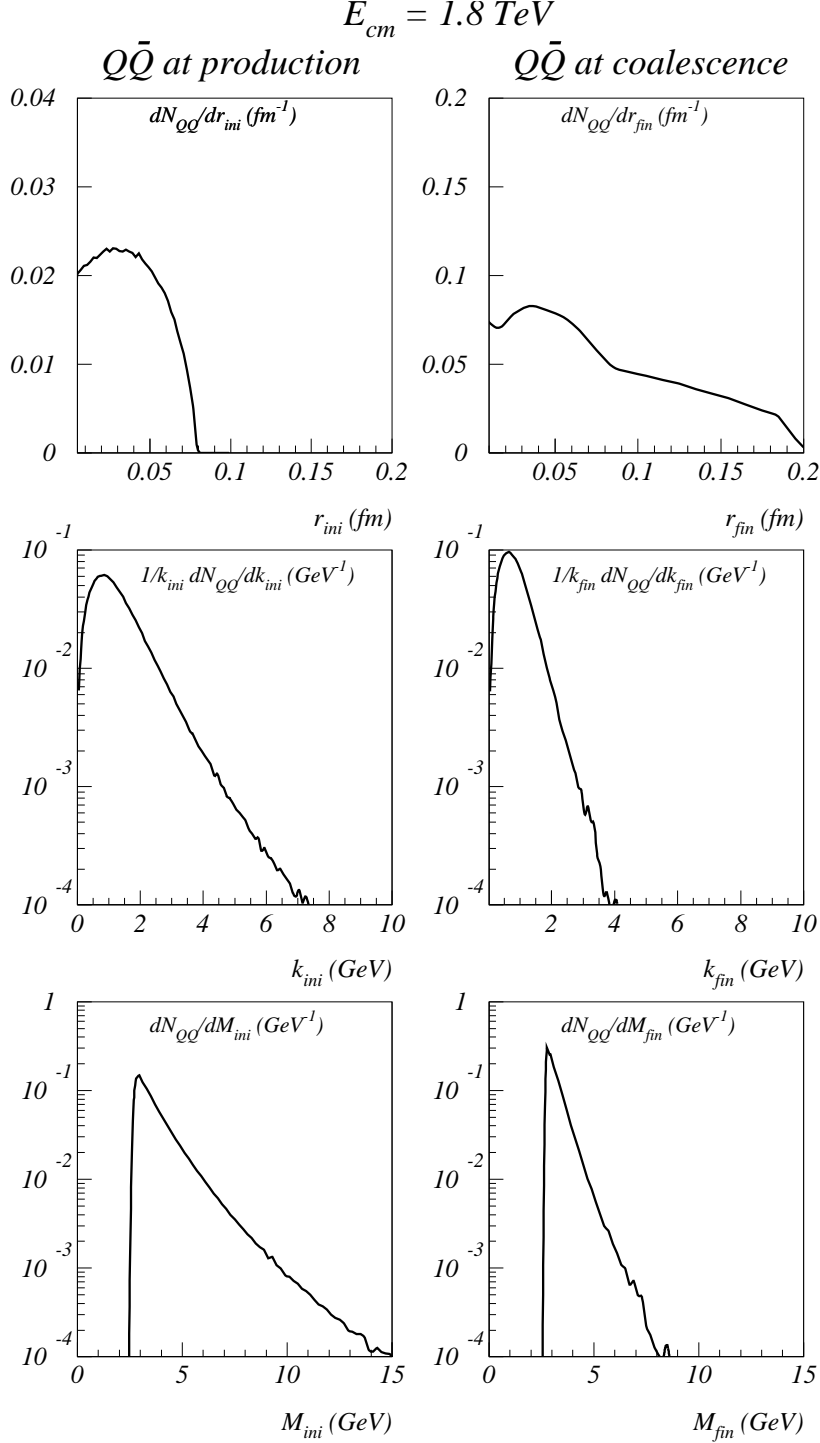


FIG. 16. Characteristics of the space-time evolution reflected in initial and final  $Q\bar{Q}$  spectra, for the case of charmonium  $p\bar{p}$  center-of-mass energy of 1.8 TeV. *Left panel:* Distributions in relative separation  $r_{ini} = |\mathbf{r}_Q - \mathbf{r}_{\bar{Q}}|_{t=t_0}$  relative momentum  $k_{ini} = |\mathbf{k}_Q - \mathbf{k}_{\bar{Q}}|_{t=t_0}$  and invariant mass  $M_{ini} = \sqrt{(k_Q^\mu + k_{\bar{Q}}^\mu)^2}|_{t=t_0}$  of the *initial*  $Q\bar{Q}$  pair upon production at  $t = t_0$ . *Right panel:* Distributions in the corresponding quantities  $r_{fin}$ ,  $k_{fin}$ ,  $M_{fin}$  of the *final*  $Q\bar{Q}$  pair upon coalescence.

## IV. CONCLUDING REMARKS AND OUTLOOK

### A. Summary

The scope of this work concerned the development and application of a space-time description for the production of heavy quarkonium as  $Q\bar{Q}$  bound-states in hadron-hadron collisions. The theoretical framework was developed on the basis of the common factorization assumption of short-distance PQCD production and evolution of heavy  $Q\bar{Q}$  pairs and the long-distance bound-state formation process leading to final-state quarkonia.

The separation of perturbative and non-perturbative momentum scales (and space-time scales) was exploited to formulate the dynamics of quarkonium production and the associated cross-section as the product of three functions corresponding to  $Q\bar{Q}$  production, parton cascade evolution, and coalescence, respectively. The practical calculation involved three corresponding elements: firstly, the ‘hard’ production of the initial  $Q\bar{Q}$ , directly or via gluon fragmentation and including both color-singlet and -octet contributions, secondly, the subsequent development of the  $Q\bar{Q}$  system within a space-time generalization of the DGLAP parton-evolution formalism in position- and momentum-space, and thirdly, the actual formation of the bound-states being described by the space-time dependent overlap between the  $Q\bar{Q}$  pair and the spectrum of quarkonium wave-functions.

This approach was then applied to  $pp$  ( $p\bar{p}$ ) collisions in the energy range  $\sqrt{s} = 30 \text{ GeV} - 14 \text{ TeV}$ , corresponding to the range of center-of-mass energies between ISR, Tevatron, and LHC experiments, by simulating the space-time development of the complete particle system of a collision event, using a suitably extended version of the computer program VNI. Comparison with experimental data from ISR and Tevatron for both charmonium and bottomonium production revealed very good agreement of the model calculations, essentially without the necessity of introducing tunable, free parameters. Details of the underlying dynamics that lead to the decent *postdictions* of ISR and Tevatron data (and *predictions* for LHC), were analyzed in particular with respect to the relevance of gluon radiation, the contributions of color-singlet and color-octet  $Q\bar{Q}$  systems, and the characteristics of the space-time structure.

### B. Future perspectives

Finally some remarks on future perspectives. The good agreement with available experimental data of the present approach to quarkonium production in  $pp$  or  $p\bar{p}$  collisions, as well as its transparent physics concept, suggests to extend applications and tests of the model to other collision systems.

- *pion-proton collisions* are experimentally well studied too in terms of quarkonium production (although at lower energies), observed with even distinctly larger yields, partly due to the different valence quark content of the initial state. It would be interesting to test whether the model advertized here is capable of describing these reactions equally well.
- *proton-nucleus collisions* are another extension for which again quite some experimental data exist for various energies and different nuclei. The novel feature here, as compared to hadron-hadron collisions, is the propagation of the  $Q\bar{Q}$  pair in nuclear matter, that is, before forming a bound-state,  $Q$  and/or  $\bar{Q}$  may experience scatterings off partons belonging to close-by nucleons in the traversed nucleus. As a consequence, one expects the quarkonium yield to be reduced due to the deflection of  $Q$  and/or  $\bar{Q}$  and the resulting failure of coalescence.
- *nucleus-nucleus collisions*, finally, are a most interesting ground for studying quarkonium production in QCD matter, in particular since it has become appreciated as one of the best experimental probes for indirect detection of a quark-gluon plasma, a high-density and high-temperature state of deconfined partonic matter for which first hopeful signals have been extracted recently in lead-on-lead collisions at the CERN SPS facility. Compared to proton-nucleus collisions, in heavy-ion reactions several new physics issues arise. For example, the large size of the nuclear collision system makes it likely that the traversed distance of a heavy  $Q\bar{Q}$  system can extend over several  $fm$  so that not only the  $Q$  and  $\bar{Q}$  are likely to re-interact before they may coalesce, but also the coalesced  $Q\bar{Q}$  bound-states can re-collide and being broken up again (so-called ‘dissociation’). Moreover, in central collisions of heavy nuclei at sufficiently large energy per nucleon, it is expected [24] that copious parton materialization and mini-jet production through very frequent parton collisions, plus further parton multiplication through gluon emission induced by partonic re-scatterings, may create very quickly (within a fraction of a  $fm$ ) a very dense and highly excited partonic environment. Whether or not this QCD matter approaches an equilibrium state, i.e. some sort of quark-gluon plasma, the properties of the hot and dense parton matter are of their own fundamental interest. In this context, quarkonium production is certainly a pre-destined probe to study these properties, as mentioned before. Both the yield of formed  $Q\bar{Q}$  bound-states and the survival probability of resulting quarkonium states are likely to be suppressed, the degree of suppression being an indicator of the

density and temperature of the nuclear matter. It is clear that here the space-time picture is an inevitable necessity to study quarkonium production in high-density QCD, where accounting for the dynamically evolving space-time structure of the collisions is most important, and where the time-dependent spatial profile of the particle density is the key quantity that determines the fate of quarkonium. Since the local density is created by the interrelated space-time structure of many parton cascades evolving close-by in the central collision region, it the only way of ‘calculating’ the dynamics is by rigorous accounting for both the space-time variables and the energy-momentum variables for each particle present at a given time during the collision. Here lies a real challenge for the model advocated in this paper. The technicalities of extending the present status to nuclear collisions are straightforward, though non-trivial, and work is in progress.

## ACKNOWLEDGEMENTS

This work was to large extent inspired and driven by numerous discussions with Sidney H. Kahana and David E. Kahana, who also were involved in a revision of an initial draft of the manuscript. Thank you very much. Furthermore, I would like to thank Eric Braaten for guidelining suggestions, and Michelangelo Mangano for encouragement as well as supplying the Tevatron data in ready-to-plot format. This work was supported in part by the D.O.E under contract no. DE-AC02-76H00016.

## REFERENCES

- 
- [1] C. Albajar *et al.* (UA5), Phys. Lett. **B256**, 112 (1991).  
F. Abe *et al.* (CDF), Phys. Rev. Lett. **69**, 3704, (1991); **71**, 2357, (1992); **75**, 1451, (1995); FERMILAB-PUB-97/024 (unpublished); FERMILAB-PUB-97/026-E (unpublished).  
K. Bazizi (D0), in the *Proceedings of the X'th Topical Workshop on  $p\bar{p}$  Physics*, Fermilab publication 1995.
  - [2] M. Gonin, Nucl. Phys. **A610**, 404c (1996).
  - [3] M. Mangano, in the *Proceedings of the X'th Topical Workshop on  $p\bar{p}$  Physics*, Fermilab publication 1995 (hep-ph/9507353).
  - [4] E. Braaten, S. Fleming, and T. C. Yuan, Ann. Rev. Nucl. Part. Sci. **47**, 197 (1997).
  - [5] S. Frixione, M. Mangano, P. Nason, and G. Ridolfi, preprint CERN-TH/97-16 (hep-ph/9702287).
  - [6] D. Kharzeev and H. Satz, Nucl. Phys. **A590**, 515c (1995); D. Kharzeev, Nucl. Phys. **A610**, 418c (1996).
  - [7] B. Guberina, J. H. Kühn, R. D. Peccei, and R. Rückl, Nucl. Phys. **B174**, 317 (1980).
  - [8] R. Baier and R. Rückl, Z. Phys. **C19**, 251 (1983).
  - [9] R. Gastmans, W. troost, and T. T. Wu, Nucl. Phys. **B291**, 731 (1987).
  - [10] G. Schuler, preprint CERN-TH-7170-94, to appear in Phys. Rept. (hep-ph/9403387).
  - [11] G. T. Bodwin, E. Braaten, and G. P. Lepage, Phys. Rev. **D51**, 1125 (1995).
  - [12] M. Beneke, preprint CERN-TH/97-55 (hep-ph/9703429).
  - [13] C. Quigg and J. L. Rosner, Phys. Rept. **56**, 168 (1979).
  - [14] E. Eichten, K. Gottfried, T. Kinoshita, K. D. Lane, and T.-M. Yan, Phys. Rev. **17**, 3090 (1978).
  - [15] P. Cho and A. K. Leibovich, Phys. Rev. **D53**, 150 (1996); **D53**, 6203 (1996).
  - [16] E. Braaten and Y.-Q. Chen, Phys. Rev. Lett. **76**, 730 (1996);  
P. Cho and A. K. Leibovich, Phys. Rev. **D54**, 6690 (1996) **D53**, 6203 (1996).
  - [17] M. Cacciari and M. Greco, Phys. Rev. Lett. **73**, 1586 (1994);  
E. Braaten, M. A. Doncheski, S. Fleming, and M. Mangano, Phys. Lett. **B333**, 548 (1994);  
D. P. Roy and K. Sridhar, Phys. Lett. **B339**, 141 (1994);  
M. Cacciari, M. Greco, M. Mangano, and A. Petrelli, Phys. Lett. **B356**, 553 (1995).
  - [18] H. Fritzsch, Phys. Lett. **67**, 217 (1977).

- [19] L. N. Lipatov, Sov. J. Nucl. Phys. **20**, 94 (1975);  
Yu. L. Dokshitzer, Sov. Phys. JETP **46**, 641 (1977);  
G. Altarelli and G. Parisi, Nucl. Phys. **B126**, 298 (1977).
- [20] K. Konishi, A. Ukawa, and G. Veneziano, Nucl. Phys. **B157**, 45 (1979);  
Yu. L. Dokshitzer, D. I. Dyakonov, and S. I. Troyan, Phys. Rep. **58**, 269 (1980);  
A. Bassetto, M. Ciafaloni and G. Marchesini, Phys. Rep. **100**, 203 (1983).
- [21] D. E. Kahana, S. H. Kahana, Y. Pang, A. J. Baltz, C. B. Dover, E. Schnedermann, and T. J. Schlagel, Phys. Rev. **C54**, 338 (1996);  
C. B. Dover, U. Heinz, E. Schnedermann, and J. Zymnanyi, Phys. Rev. **C44**, 338 (1991).
- [22] See, e.g.: K. Hamacher and M. Weierstall, Preprint DELPHI 95-80 PHYS 515 (hep-ex/9511011).
- [23] K. Geiger, preprint BNL-63632, hep-ph/9701226 (to appear in Comp. Phys. Com.).
- [24] K. Geiger, Phys. Rept. **258**, 238 (1995).
- [25] K. Geiger, Phys. Rev. **D47**, 133 (1993).
- [26] Yu. L. Dokshitzer, V. A. Khoze, A. H. Mueller, and S. I. Troyan, Rev. Mod. Phys. **60**, 373 (1988).
- [27] See e.g.: J. J. Sakurai, *Modern Quantum Mechanics*, (Addison-Wesley, 1985).
- [28] Ya. I. Azimov, Yu. L. Dokshitzer, V. A. Khoze and S. I. Troyan, Z. Phys. **C27**, 65 (1985); Yu. L. Dokshitzer, V. A. Khoze and S. I. Troyan, Z. Phys. **C55**, 107 (1992).
- [29] Yu. L. Dokshitzer, V. A. Khoze, and S. I. Troyan, Phys. Rev. **D53**, 89 (1996).
- [30] E. Eichten and C. Quigg, Phys. Rev. **D52**, 1726 (1995).
- [31] M. Glück, E. Reya and A. Vogt, Z. Phys. **C48**, 471 (1990); Z. Phys. **C67**, 433 (1995).
- [32] J. Ellis and K. Geiger, Phys. Rev. **D54**, 949 (1996); Phys. Rev. **D54**, 1755 (1996).
- [33] See e.g.: Particle Data Group, *Review of Particle Properties*, Phys. Rev. **D50**, 1173 (1994).
- [34] A. G. Clark *et al.*, Nucl. Phys. **B142**, 29 (1978);  
K. Ueno *et al.*, Phys. Rev. Lett. **42**, 486 (1979);  
C. Kourkoumelis, *et al.*, Phys. Lett. **B91**, 405 (1980); Phys. Lett. **B91**, 481 (1980).